Final Master Project

DEVELOPMENT AND OPTIMIZATION OF CATALYSTS FOR ENHANCED METHANE NON-OXIDATIVE COUPLING PROCESSES.

Nidya Lara Rico

Supervisors:

Dr. Ignacio Julián
Dr. Scott G. Mitchell
Dr. José Luis Hueso

Facultad de Ciencias
2018

ACKNOWLEDGMENTS

ABSTRACT

Dehydroaromatization of methane (MDA) is a promising reaction to directly convert methane into aromatics and hydrogen. MDA is an endothermic reaction and, accordingly, it requires high temperatures in combination with selective catalysts to obtain a sufficient yield of aromatics, specially bezene. The benchmark catalyst for this reaction is Mo/zeolite, it form of 10-membered ring zeolites (such as HZSM-5 and H-MCM-22) for their high activity and aromatic selectivity, but the main drawback of this reaction is the rapid deactivation of catalyst due to the formation of coke on its surface.

The present research word project is focused on the synthesis and development of catalysts that are active, stable and selective for the non-oxidative coupling of the methane reaction (MNOC), and then optimize them in a conventional oven to generate light aromatic hydrocarbons, preferentially benzene.

A selection of polyoxomolybdate anions were used as the Mo source with the hypothesis that the different structural arrangement of their Mo atoms within the polyoxometalate (POM) molecules would help to generate repulsion between discrete Mo centres, thereby avoiding the formation of Mo agglomerates on the zeolite surface.

Zeolitic supports ZSM-5 and MCM-22 were used to support different loadings of Mo from three different types of polyoxomolybdate anion. The catalysts were tested for MNOC reaction under conventional heating and the catalysts prepared with the "Mo6" precursor, especially the 5% Mo6/MCM-22, showed an excellent stability with 22 hours of reaction and an optimum yield to benzene.

TABLE OF CONTENTS

1. INTRODUCTION

Worldwide energy demand is increasing rapidly and, despite the discovery of new oil fields, the excess consumption of this type of fossil fuel remains problematic. The depletion of reserves and inaccessibility of the remaining deposits will inevitably lead to a large increase in the cost of this raw material. Over the last several decades, researchers have focused a great deal of effort into the development of new technologies that allow maintaining the current energy regime, to obtain the same primary compounds that were derived from petroleum. One of the most promising energy sources is methane that is extracted in the form of natural gas from subsoil deposits. Natural gas is frequently found in fossil deposits, alone or accompanying an oil or coal deposit, although it can also be obtained through decomposition processes of organic waste (biomass). The huge reserves, its potential contribution to improved environmental sustainability, and lower overall costs point to natural gas as the dominating primary source for energy and chemicals in the near future [1]. Among the fossil fuels, natural gas provides the lowest environmental penalty, i.e. its combustion produces the lowest amount of particulate matter and sulfur dioxide. Nevertheless, an important amount of the proven reserves of natural gas is located at small and medium reservoirs in remote regions. Due to the gaseous nature of this energy source, its transportation to end-users requires either the construction of pipelines or its confinement into the so-called liquefied natural gas (LNG). Neither of these alternatives are economically feasible for small and medium-scale reservoirs. A promising alternative to exploit these deposits consists in performing an in-situ conversion of natural gas into added-value chemicals, e.g. olefins, oxygenated derivatives or liquid hydrocarbons. Natural gas is a variable mixture of light hydrocarbons which composition varies according to the deposit. In any case, its main component is methane, which usually becomes between 80 and 97% of the total volumetric composition of natural gas [2, 3]. The rest is essentially composed of compounds such as ethane, propane, butane, nitrogen or carbon dioxide. This diversity creates a need to develop modular, flexible catalytic reactor systems capable of valorizing methane to longer hydrocarbons and of operating with changing methane feedstocks in various environments. This represents the main motivation of the European Project ADREM (*"Adaptable reactors for the resource- and energy-efficient methane valorization"*), which hosts this research work.

1.1. Valorization of methane

The transformation of methane into heavy hydrocarbons of higher molecular weight and greater added value is a scientific and technological challenge that has been studied since the second half of the 20th century. The major drawback has been the great stability and low reactivity that the methane molecule exhibits. This is due to the tetrahedral arrangement of its covalent hydrogen-carbon bonds (d C-H = 1.09 Å) with bond energy of 413 kJ/mol. This molecule offers no functional group, magnetic moments or polar distributions to carry out a chemical attack [4]. Methane activation, i.e. C-H bond cleavage, requires high temperatures and, as a result, a high energy demand. For this reason, it is essential to use a catalyst that is capable of decreasing the activation energy of the reaction. The existing methane conversion routes towards higher hydrocarbons are classified into two routes in heterogeneous catalysis:

1. **Indirect routes**: those where the methane transformation into high value-added products requires at least two stages. In the first one, methane is converted into synthesis gas (mixture of CO and H$_2$) whereas in further stages the mixture is transformed into the desired final products via Fischer-Tropsch process [5]. The indirect transformation of methane produces remarkable yields but the process is quite costly and its feasibility is restricted to large-scale productions.

2. **Direct routes**: methods to obtain the products of interest through one-step conversion of methane. These routes imply cost reductions derived from equipment and maintenance with respect to indirect ones. Nevertheless, their production yields are still substantially lower and this hinders their implementation at the industrial level.

Among the direct routes, the non-oxidative catalytic conversion of methane (hereafter MNOC) into added-value aromatics and olefins, i.e. benzene, naphthalene and ethylene, is a very promising route for methane valorization [6,7]. However, the heterogeneous catalytic conversion of methane presents several limitations. On the one hand, methane conversion has thermodynamic restrictions and it becomes negligible at temperatures below 650ºC. On the other hand, high temperatures promote the decomposition of methane into heavy carbonaceous deposits (coke) on the catalyst surface that drastically decreases methane conversion along the time on stream.

Therefore, research efforts are devoted primarily to improving catalyst stability, i.e. coke resistance, and to enhancing overall conversion and hydrocarbon selectivity.

1.2. Overview of the catalysts for non-oxidative routes for methane conversion
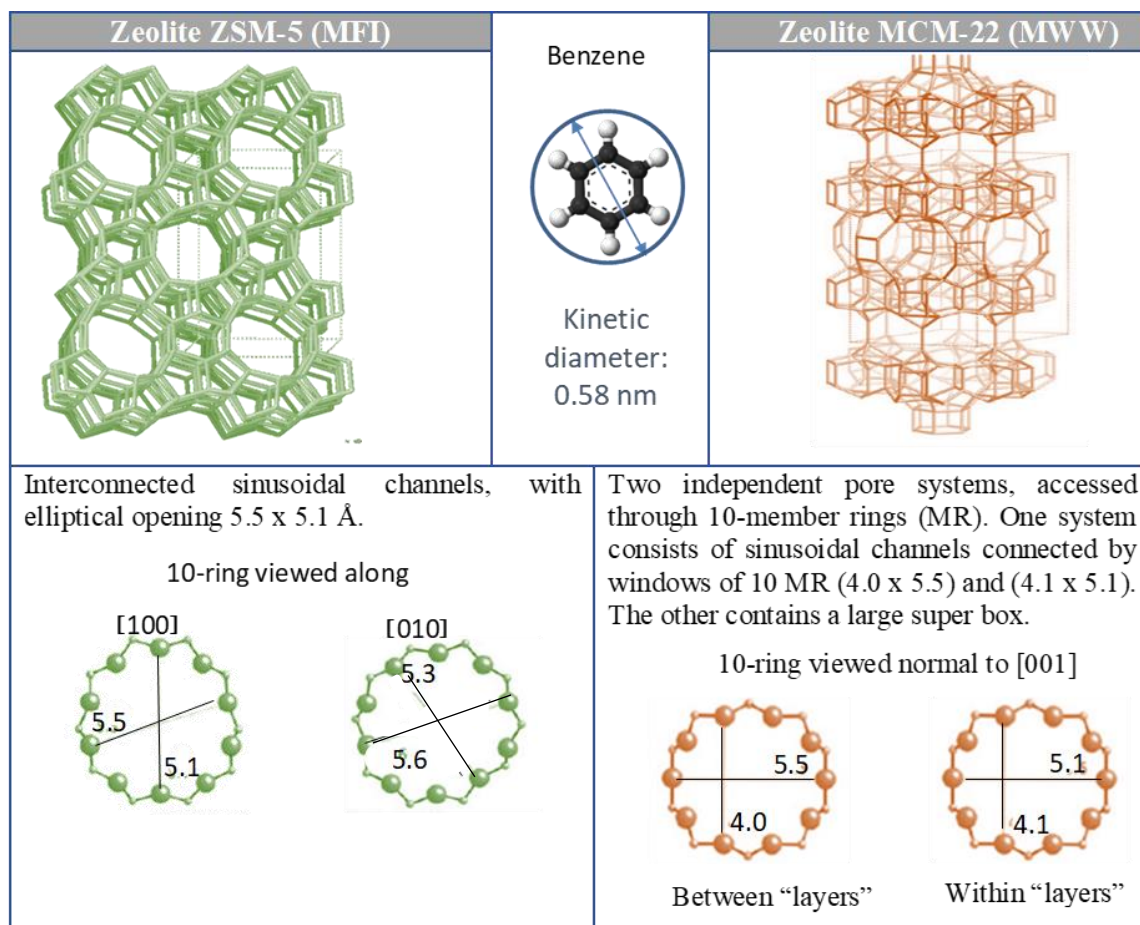
Figure 1. The main characteristics of the zeolites used as support in the synthesis of the catalysts

To carry out the dehydrogenation reaction, catalysts with surface-active centers of an acid nature are required. Previous studies indicate that aluminosilicate zeolite ZSM-5 contains strong Brönsted acid sites, and is therefore an effective catalyst for this type of transformations, providing a shape-selective environment for the conversion of methane to benzene. However, deactivation induced by coke formation leads to a decrease in activity and selectivity towards light aromatics such as benzene and therefore makes the process unsuitable for large-scale industrial applications. Figure 1 shows two types of zeolitic materials and describes their main characteristics

In general, Mo/MCM-22 seems to increase the benzene-to-naphthalene yield ratio in comparison to Mo/ZSM-5 under the same experimental conditions, due to its unusual

channel structure. Notwithstanding, for the reaction under non-oxidative condition, usually MCM-22 is less preferred than ZSM-5, due to its lower commercial availability and complex synthesis procedure [8].

1.3. Polyoxometalates (POMs) and their application in catalysis

As described above, in this work the use of polyoxomolybdates as Mo precursors in the preparation of Mo / ZSM5 and Mo / MCM-22 catalysts is proposed in order to increase the Mo dispersion and improve the catalytic activity and the resistance from the catalyst to the coke. Polyoxometalates (POMs) are a large family of anionic metal-oxide clusters of early row transition metals - typically W, Mo and V - in their highest oxidation state. These nanoscale molecular metal oxides have aroused great interest due to their highly applicable catalytic properties [9]. They possess high thermal stability, are strong Brönsted acids and readily undergo redox reactions without changes to their structural composition. In their highest oxidation state atoms of molybdenum and tungsten possess empty d orbitals and a favorable ionic radius, which facilitate π metal-oxygen overlap [10]. They can be grouped into two main groups: isopolyoxometalates and heteropolyoxometalate.

The isopolyanions are those that contain only one transition metal atom type (M) bonded with oxygen and are generally expressed as $[M_mO_y]^{n-}$.. These are formed by condensation of octahedral MO_6 that share edges and vertices. The six oxygen atoms that make up each octahedron are not equivalents so all the octahedrons will be deformed. On the other hand, a heteropolyanion will be one in which an atom different of a transition metal is introduced in the voids that are formed by the condensation of the octahedra. The atom that occupies that cavity is called heteroatom and is usually Si, Ge or P. The heteroatom is, therefore, coordinated to the oxygens that surround it and becomes part of the polyoxoanion structure. POMs have many interesting applications: as catalysts (homogeneous and heterogeneous), they are widely used, both in redox reactions, for their flexibility and capacity to accept and donate electrons, and in acid-base catalysis, due to their strong acid character [11,12]. Recently, several POMs with multiple d-electron transition metal centers have proved to constitute of a novel class of soluble, carbon-free molecular catalysts that integrate both high efficiency and robustness in one structure. In addition, these compounds have advantages as catalysts because they are economically and environmentally attractive.

2. MOTIVATION OF THE PROJECT AND OBJECTIVES

2.1. Framework of this Project

This project is part of the European project ADREM ("Adaptable reactors for the valorization of methane of resources and efficient energy"), focused on the intensification of processes for the efficient valuation of natural gas. The ADREM project (E.U. Horizon 2020) aims to develop a highly innovative, economically attractive and energy-efficient recovery process of variable raw materials, from methane to higher hydrocarbons and liquid fuels, through the development of energy-efficient reactors for valorizing methane [1]. To achieve this, it is first necessary to develop catalysts that are active, stable and selective for the non-oxidative coupling of the methane process, and then optimize them in a conventional oven to generate light and aromatic hydrocarbons as value-added products for the energy and petrochemical industries. A literature review showed which materials were the best options to use as precursors and supports for the development of catalysts for the non-oxidative coupling of methane. These reports showed that the catalyst Mo/ZSM-5 offered the best results in terms of benzene selectivity; however, they also report some of the limitations that occur in non-oxidative methane coupling reactions such as the deactivation of the catalyst over time in the stream due to the formation of heavy carbonaceous deposits on the surface of the catalyst [3-5].

One of the reasons why the formation of the coke can take place is due to the non-uniformity of the Mo dispersion on the surface of the support at the time of impregnation, which leads to the formation of molybdenum aggregates, that after the calcination process these are converted into large crystals of molybdenum oxide that clog the pores of the zeolite. Therefore, POMs are excellent candidates as Mo precursors, due to the structural arrangement of their molecules that have a metallic center surrounded by oxygen atoms, which generates repulsion between discrete anions, helping to avoid the formation of agglomerates. This would be a great advantage to use POMs as Mo precursors since when doing the impregnation, it would help us to have a better dispersion of Mo in the surface of the support, so the formation of coke in the reaction would be reduced which benefits activating the catalyst for longer.

2.2. Objectives

The overall aim of this project is to explore different types of Mo-containing Zeolitic catalysts to perform the selective non-oxidative coupling of methane (MNOC) to transportable aromatic hydrocarbons. To achieve this objective various types of polyoxomolybdate precursors will be synthesized and embedded in two types of Zeolitic frameworks (H-ZSM-5, MCM-22). The stability and selectivity of these catalysts towards benzene by the non-oxidative coupling of methane will then be evaluated in a reactor operated by an electric furnace. Consequently, the final aim is to determine the most effective Mo loading and catalyst combination to further optimize the MNOC reaction.

3. EXPERIMENTAL PROCEDURE

This section details the synthesis routes to obtain the Mo precursors (POMs) and the Mo/ZSM-5 and Mo/MCM-22 catalysts as well as the techniques used to characterize the prepared samples. Subsequently, the experimental plant used to test the catalysts and the battery of reaction tests carried out according to the different operating variables will be described.

3.1. Mo precursors synthesis: POMs

When talking about synthesis in aqueous solutions it is possible to make a classification: synthesis from starting reagents, or synthesis from other polyoxoaniones, called resources.

As our objective is to synthesize simple polyoxometalates such as $[Mo_6O_{19}]^{2-}$ ("Mo$_6$") and $[Mo_8O_{26}]^{4-}$ ("Mo$_8$"). We will use basic alkaline salts like Na_2MoO_4 and $[(n-C_4H_9)_4N]Br$ are used as starting materials. Because of this, large amounts of sodium salts are produced as byproducts.

3.1.1. Synthesis of tetrabutylammonium hexamolybdate (VI), $[(n-C_4H_9)_4N]_2(Mo_6O_{19})$, "Mo$_6$"

$$6Na_2MoO_4 + 10HCl + 2(n-C_4H_9)_4NBr \longrightarrow [(n-C_4H_9)_4N]_2(Mo_6O_{19}) + 10NaCl + 2NaBr + 5H_2O$$
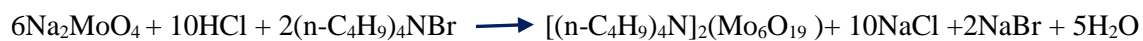
In an Erlenmeyer was prepared a solution with 10 g of $Na_2MoO_4.2H_2O$ in 40 mL water (acidified with 11.6 mL of 6 N HCl), this solution was on vigorous stirring over a 1 minute at room temperature. After that a solution of 4.84 g of (n-C$_4$H$_9$)$_4$NBr in 8 mL of water was added with vigorous stirring to cause the formation of a white precipitate. The resulting slurry was heated to 75 to 85, stirring for 45 minutes the white solid slowly changed to yellow. This yellow solid was filtered and washed thrice with 80 mL of water.

Crystallization was accomplished by dissolving the dried crude product in 80 mL of hot acetone 60 °C and cooling the solution to –20 °C. After 24 h, the yellow crystalline products were collected on a filter with suction, washed twice with 20 mL of diethyl ether and dried for 12 h in vacuum.

3.1.2. Synthesis of tetrabutylammonium octamolybdate (VI), [(n-C₄H₉)₄N]₄[Mo₈O₂₆] "Mo₈"

$$8Na_2MoO_4 + 12HCl + 4[(n\text{-}C_4H_9)_4NBr] \longrightarrow [(n\text{-}C_4H_9)_4N]_4[Mo_8O_{26}] + 12NaCl + 4NaBr + 6H_2O$$
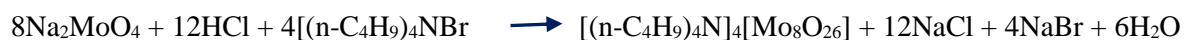
A solution of 10 g of commercial, ACS reagent grade, sodium molybdate dehydrate in 24 mL water was acidified with 10.4 mL of 6.0 N aqueous HCl in a 100 mL Erlenmeyer with vigorous stirring over a period of 2 minutes at room temperature. A solution of 6.68 g of commercial 99% pure tetrabutylammonium bromide in 20 mL of water was then added dropwise with vigorous stirring to cause the immediate formation of a white precipitate.

After stirring the mixture for 15 min, the precipitate was separated by centrifugation and it was washed 30 mL of water, was centrifuged again, and next was washed with acetone (until the washings are clear, not yellow), then with 60 mL of ethanol and 60 mL diethyl ether. The white powder obtained was dried in freeze dryer. Figure 2, shows the three types of precursors that were used for the synthesis of the catalysts.
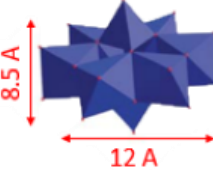
POMs synthesized		Commercial salt
Tetrabutylammonium hexamolybdate (VI) **"Mo₆"**	Tetrabutylammonium octamolybdate (VI) ''Mo₈''	Ammonium molybdate tetrahydrate ''Mo₇''
$[Bu_4N]^+[Mo_6O_{19}]^{2-}$	$[Bu_4N]^+[\alpha\text{-}Mo_8O_{26}]^{4-}$	$[NH_4]^+[Mo_7O_{24}]^6$

Figure 2. Molybdenum precursors used for the synthesis of catalysts

3.2. Support synthesis: MCM-22.

The zeotype MCM-22 was synthesized following the procedure reported by Corma *et al* [13] using hexamethyleneimine (HM) as a large molecule that acted as the structure directing agent (OSDA). Crystallization was carried out in a stainless steel Teflon-lined autoclave at 423 K, under agitation (60 rpm) and autogenous pressure for 7 days. After this period, the solid was recovered by filtration, washed repeatedly with deionized water, and dried overnight at 393 K, followed by calcination in air at 823 K for 5 h to remove the occluded organic SDA in the inner pores. The zeolitic material was refluxed in 1.0 M NH_4NO_3 solution to exchange the Na^+ by NH_4^+ and finally calcined at 823 K for 5 h. This procedure was repeated twice in order to obtain the sample in its acid form. At the time of characterization by XRD (Figure 3), the most characteristic peaks coincided with these of the MCM-22 structure [13-14].
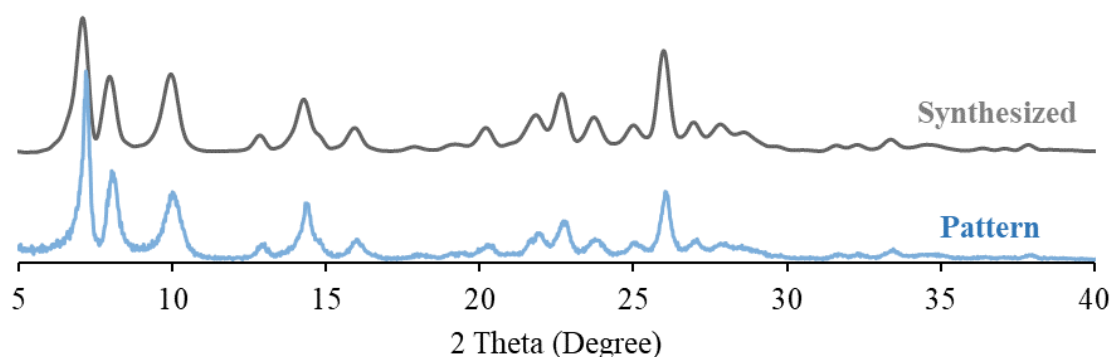
Figure 3. X-ray diffraction spectra MCM 22 of pattern and the sample synthesized.

3.3. Synthesis of catalysts for methane activation: Mo_x/ZSM-5 and Mo_x/MCM-22.

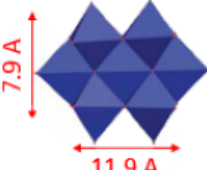Mo_x/ZSM-5 and Mo_x/MCM-22 catalytic powders were prepared using three different molybdenum precursors, of which two were synthesized (tetrabutylammonium hexamolybdate (VI) $[Bu_4N]^+$ $[Mo_6O_{19}]^{2-}$ and tetrabutyl ammonium octamolybdate (VI) $[Bu_4N]^+$ $[\alpha\text{-}Mo_8O_{26}]^{4-}$ ("Mo_8") and the other was purchased from Sigma-Aldrich CAS Number 12054-85-2 (ammonium molybdate tetrahydrate $[Mo_7O_{24}]^{4-}$ ("Mo_7")).

These precursors were supported on zeolite ZSM-5 ($SiO_2/Al_2O_3 = 23$) and MCM-22 ($SiO_2/Al_2O_3 = 20$) as support. The support the MCM-22 has been synthesized in the laboratories of the NFP group. All the reagents were used as purchased.

The catalysts were prepared using the method of impregnation of incipient humidity (see Figure 4), which consists of dissolving the precursor in a solvent and adding this solution drop by drop into the zeolite, under continuous mixing until reaching incipient wetness. The resulting materials were dried at 120°C overnight and calcined at 550°C for 6 h, using a heating rate of 1°C /min. These calcination parameters were previously determined by an assay that is explained in Chapter 4.1. In order to corroborate what has been mentioned in other works on the influence of the calcination temperature in the formation of different species of molybdate in the catalysts, as explained in the following section.

The catalysts prepared by the impregnation method are shown in table 1.

a. Mo_6 solution.

b. Mixture of zeolite with Mo_6 solution

c. Under continuous mixing until incipient wetness achieved.

d. Heating ramp (dried and calcined)
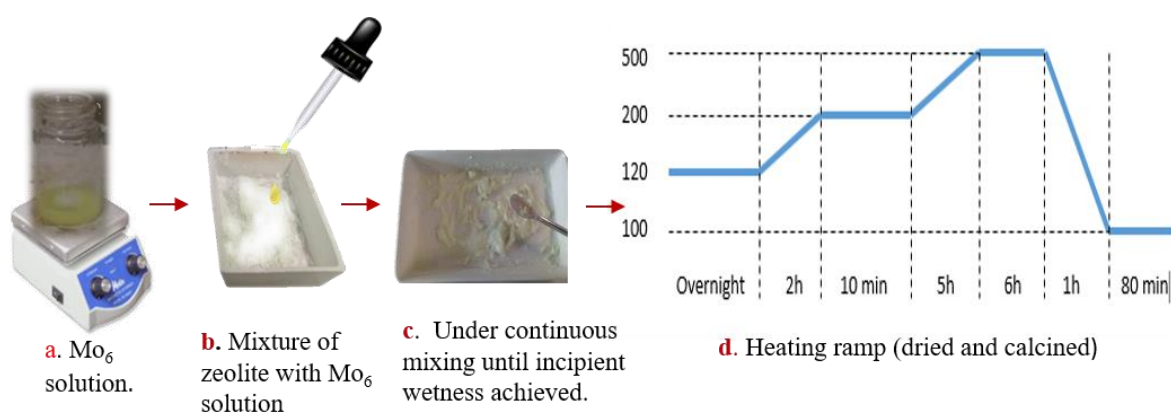
Figure 4. Diagram of catalyst synthesis by impregnation of incipient humidity

Table 1. Summary of synthesized catalysts, indicating the employed precursor, metal load and support used.

Support	Precursor	Metal load (wt%)	Code
ZSM-5	$[(C_4H_9)_4N]_2$ (Mo_6O_{19})	5	5% Mo_6/ZSM-5
	$(NH_4)_6Mo_7O_{24} \cdot 4H_2O$		5% Mo_7/ZSM-5
	$[(C_4H_9)_4N]_4$ Mo_8O_{26}		5% Mo_8/ZSM-5
MCM-22	$[(C_4H_9)_4N]_2$ (Mo_6O_{19})	5	5% Mo_6/MCM-22
		8	8% Mo_6/MCM-22
		10	10% Mo_6/MCM-22
	$(NH_4)_6Mo_7O_{24} \cdot 4H_2O$	5	5% Mo_7/MCM-22

3.3.1. Effect of calcination temperature on Mo / ZSM5 catalyst

As mentioned above, previous works have demonstrated that the heating ramp and calcination temperature during the calcination process play a key role in the obtaining of different Mo species, which affect the final performance of the Mo-based catalyst under the

MDA reaction [2, 3, 5]. At a calcination temperature of 500 °C, it is most likely that the catalyst is oxidizing into crystalline MoO_3 species that remain on the outer surface as molybdenum oxide particles. However, at temperatures of 550 °C or above, MoO_3 species seem to diffuse into to zeolite channels and exchange with OH groups in the ZSM-5 framework to form dimers $(Mo_2O_5)^{2+}$ anchored in two cation exchange sites [2,5] as depicted in Figure 5.
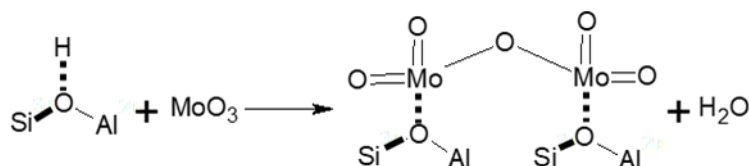
Figure 5. Solid Exchange of MoO_3 with OH groups of zeolite [3]

So, the most likely that during the CH_4 reactions, theses OH bonds are regenerated by the reduction and carburization of the species $(Mo_2O_5)^{2+}$ causing the formation of MoC_x clusters [2, 3] (Figure 6).
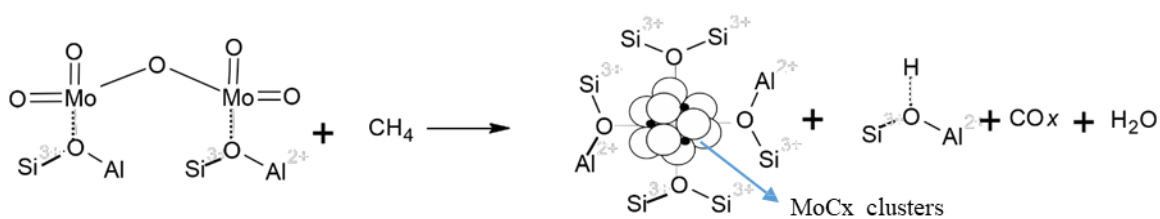
Figure 6. Reaction of Exchanged of MoO_x/H-ZSM5 with CH_4

3.4.   Characterization techniques

Summary of the different characterization techniques employed for analyzing the catalysts prepared during the experimental work. The Annex 1 - Table 1 shows a summary of the different characterization techniques employed for analyzing the catalysts prepared during the experimental work.

3.4.1.   Argon Adsorption

The study of the textural properties of the catalysts is of great importance in heterogeneous catalysis since it allows to quantify the microporosity, mesoporosity and external surface of the solid. These properties of the catalyst are of vital importance in understanding the catalytic behavior of the solid in relation to its channel system and its adsorption / diffusion capacity. These measurements allow to quantify the specific surface, the volume of pore and the distribution of said volume in porous solids.

So, to study the textural properties of the zeolite based catalysts evaluating the characteristic argon adsorption isotherm. The measurements were carried out using a Micrometrics ASAP 2020 analyzer. Samples were degassed at 350 ºC prior to the analysis. The determination of the specific surface has been made using the equation proposed by Brunauer, Emmet and Teller (BET) that is based on two main hypotheses: the surface of the adsorbent is uniform and non-porous, and the gas molecules are adsorbed on successive layers, without considering the lateral interactions between the adsorbate molecules, so it is applicable only at very low relative pressures. The maximum pore volume was obtained from the Horvath-Kawazoe graph.

3.4.2. *Thermogravimetric Analysis (TGA)*

The thermal stability of polyoxometalates is very important when its application is destined to heterogeneous catalysis because the risk is run that its catalytic activity is lost by the degradation of the compound. Thus that the thermogravimetric analysis (TGA) was used to determine the changes in the mass that the POMs and catalysts undergo when heated at a programmed temperature. The gravimetric thermal differential (DTG) and TGA were studied with the Q5000SA thermal analyzer and the measurement was carried out in a nitrogen atmosphere at a heating rate of $10°C$ min^{-1} from room temperature to 900 °C.

3.4.3. *Scanning Electron Microscopy (SEM) and Energy-dispersive X-ray Spectroscopy (EDX).*

SEM was used to study the morphology of catalysts and the distribution of molybdenum on the surface of zeolite support. The scanning electron microscope (SEM) offers high-resolution images of the surface of the sample to be examined. The analyses were carried out in an INSPECT-F50 scanning electron microscope from FEI Company. The equipment uses a high resolution Schottky field emission gun and a variety of detectors. The secondary electron detector (SED), back-scattered electron detector (BSED) and energy-dispersive X-ray detector (EDS) were used to examine the morphology, to study the dispersion of molybdenum and to determine the amount of molybdenum loaded, respectively. EDX spectroscopy was used to determine the weight and atomic percentages of molybdenum loaded in the catalyst as well as the distribution of the metal into zeolite. This technique consists of the emission of photons with energies in the range of X-rays.

The characteristic characters of the objects that contain the material that can be read. In this way a chemical analysis of the elements that form it is obtained.

3.4.4. X-ray Diffraction (XRD)

XRD was employed to identify molybdenum species formed on the zeolite-based catalysts. Also to study if the structure of zeolites ZSM-5 and MCM-22 changes with the addition of molybdenum. Data were recorded on an Empyrean diffractometer from PANanalytical, operating at 45 kV and 40 mA, and using CuKα radiaton. XRD spectra were collected from $2\Theta = 10°$ to $50°$. Once the measurements were carried out, all the data were processed and analyzed using the commercial software X'Pert HighScore Plus from PANanalytical. Experimental results were compared with the XRD patterns of PDF-2 database designed for identification of inorganic materials.

3.4.5. Raman Spectroscopy

Raman spectroscopy measurements were performed to identify the presence of molybdenum species on the Mo_x/ZSM-5 and Mo_x/MCM-22 catalyst. The characterization was carried out at room temperature using an Alpha 300 Raman spectrometer from WITec. A 532 nm laser was used and a CCD camera as the detector.

3.4.6. Transmission Electron Microscopy (TEM)

In the transmission electron microscope (TEM) a thin sample is irradiated with an electron beam of uniform current density, whose energy is within the range of 100 to 200 keV. Some of these electrons are transmitted, another part is dispersed and another part gives rise to interactions that produce different phenomena such as light emission, secondary electrons and Auger, X-rays, etc. All these signals can be used to obtain information about the nature of the sample (morphology, composition, crystalline structure, electronic structure, etc).

The transmission electron microscope uses the transmission / dispersion of the electrons to form images, the diffraction of the electrons to obtain information about the crystalline structure and the emission of characteristic X-rays to know the elementary composition of the sample. For the transmission of electrons through the sample to occur, it is necessary that it be thin, that is, transparent to the electrons. It is advisable not to use samples of more than 100 nm in thickness since the smaller the thickness of the sample, the better quality of images can be obtained. Sample preparation in TEM is crucial to obtain good results. A small amount of the sample was suspended in Milli Q-water and sonicated in an ultrasonic

bath for 1 minute. A drop of this suspension was deposited onto a holey TEM grid and left to dry at room temperature.

3.4.7. *Infrared spectroscopy with Fourier transform (FTIR)*

We use FTIR to confirm the main groups of the synthesized POMs. FT-IR spectroscopy has been performed on a Jasco FT/IR-4100 spectrometer. It is a very useful analysis technique in the identification of functional groups present in organic and inorganic substances. These groups are mostly absorbent, the radiations and the exciting characteristics of their vibratory and rotational modes, which generate characteristics that allow to make some deductions about the chemical nature of the substance under study.

3.4.8. *Analysis by XPS*

The technique of X-ray photoelectron spectroscopy was used to verify the presence of the phase of molybdenum species at the surface level and the oxidation state of this metal present in the Mo_x/ZSM-5 and Mo_x/MCM-22 catalysts.

3.5. Experimental plant

The description of the experimental set-up to test the synthesized catalysts for methane non-oxidative coupling under conventional heating is shown in Figure 7.

he catalysts activity tests were carried out in a continuously fixed bed quartz tubular reactor of approximately one centimetre in internal diameter (a), loaded with 0,5 g of catalyst sample. The reactor is placed in the electric oven (b). A fed mixture of CH_4: N_2 (80: 20, with N_2 as an internal standard, i.e. inert) that is supplied by three mass flow controllers (c) (Bronkhorst 0-20 mLSTP/min), it is passed through the reactor. The catalyst is heated under reaction atmosphere up to the reaction temperature 700ºC, using a heating ramp of 20ºC/min. The selected spatial velocity for the catalytic tests was 1500 mLSTP/g_{cat}·h. The sample temperature in the electrical oven was measured and controlled with a thermocouple. This thermocouple is connected to a PID controller that regulates the degree of heating of the oven to achieve a fixed temperature in the reactor.

Through a heated pipe (230 ºC), the outlet reaction gases were conducted into a gas cromatograph (Thermo Fisher Trace 1300 with auxiliary oven Trace 1310) (d) in which 4 different columns and 3 detectors that in less than 10 minutes of analysis allow the identification and quantification of permanent gases (TCD), light hydrocarbons (FID1) and aromatics (FID2).

Methane conversion (x_{CH4}) and hydrocarbon selectivity (S_{CxHy}) were calculated using Equations 1 and 2, being $\dot{n}_i$, $\dot{V}_i$, A_i and RF_i the molar flow, volumetric flow, peak area and response factor of the species i, respectively. The response factor is the ratio between the response of a detector to a compound (peak area) and the concentration of that compound in a mixture of gases. The hydrocarbon yield (Y_{CxHy}) is defined as the product of conversion by selectivity [15].
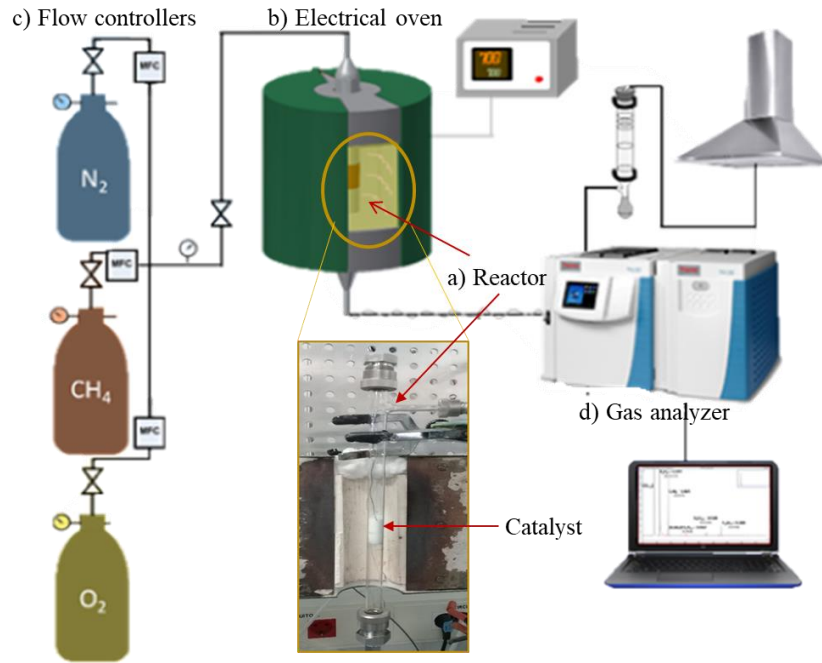
Figure 7. Set-up diagram for methane non-oxidative coupling (MNOC) tests

$$x_{CH_4} = \frac{\dot{n}_{CH_4,in} - \dot{n}_{CH_4,out}}{\dot{n}_{CH_4,in}} = \frac{\dot{V}_{CH_4,in} - \frac{A_{CH_4,out}/RF_{CH_4}}{A_{N_2,out}/RF_{N_2}}\dot{V}_{N_2,in}}{\dot{V}_{CH_4,in}} \tag{1}$$

$$S_{C_xH_y} = x \cdot \frac{\dot{n}_{C_xH_y,out}}{\dot{n}_{CH_4,in} - \dot{n}_{CH_4,out}} = x \cdot \frac{\frac{A_{C_xH_y,out}/RF_{C_xH_y}}{A_{N_2,out}/RF_{N_2}}\dot{V}_{N_2,in}}{\dot{V}_{CH_4,in} - \frac{A_{C_xH_y,out}/RF_{C_xH_y}}{A_{N_2,out}/RF_{N_2}}\dot{V}_{N_2,in}} \tag{2}$$

3.6. Reaction tests

All the reaction tests carried out in the reactor under conventional heating were carried out with the same operating conditions in order to be compared. In all of them, the operating temperature was 700 ºC, the amount of catalyst mass loaded in the reactor was 0.5 g in each test, thus, therefore, the spatial velocity was 1500 mLSTP/ g_{cat}·h since the volumetric flow

rate depends on the grams of catalyst in the reactor. The space velocity is expressed as the mL of gas entering the reactor per hour and a gram of catalyst. In this way, the inlet gas remains equal time in contact with the catalyst in each experiment, which makes it possible to compare results. All reactions were carried out with a mixture of 80% CH_4 and 20% N_2, by volume.

4. RESULTS AND DISCUSSION

To optimize the stability and selectivity of the catalysts in the valorization of methane by non-oxidative coupling, firstly, the effect of the calcination temperature at 500 and 550 ° C in the catalyst (5%Mo_7/ZSM-5) will be evaluated. The purpose is to determine what possible Mo species are formed at each temperature. Secondly, the influence of the type of molybdenum precursor (synthesized POM and commercial salt) on the ZSM-5 support will be studied evaluated to determine which catalyst has the highest selectivity to benzene and better stability under reaction conditions. After that, the effect of the zeotype support (either ZSM-5 or MCM -22) on the catalyst performance will be tested. Finally, the effect of metal loading (5-8-10% wt.) on the most promising catalyst will be discussed.

4.1. Evaluation of the effect of calcination on Mo / ZSM5 catalyst.

In order to evaluate the effect of the calcination temperature on the production of different Mo species in the calcined catalyst, the Raman spectra of two 5% Mo_7/ZSM-5 samples calcined at 500ºC and 550°C, respectively, are compared (Figure 8). The presence of the main peaks of MoO_3 (678, 829 and 1003 cm^{-1}) in the Raman spectrum of the sample calcined at 500 °C contrasts with that of the sample calcined at 550ºC, in which the peak at 960 cm^{-1} (that corresponds to $(Mo_2O_5)^{2+}$ species) becomes the most intense band. Specifically, the band at 300 cm^{-1} is attributed to the mode of bending Mo=O, to the mode of stretching from 829 cm^{-1} to Mo-O-Mo and from 1003 cm^{-1} to Mo=O of stretching,
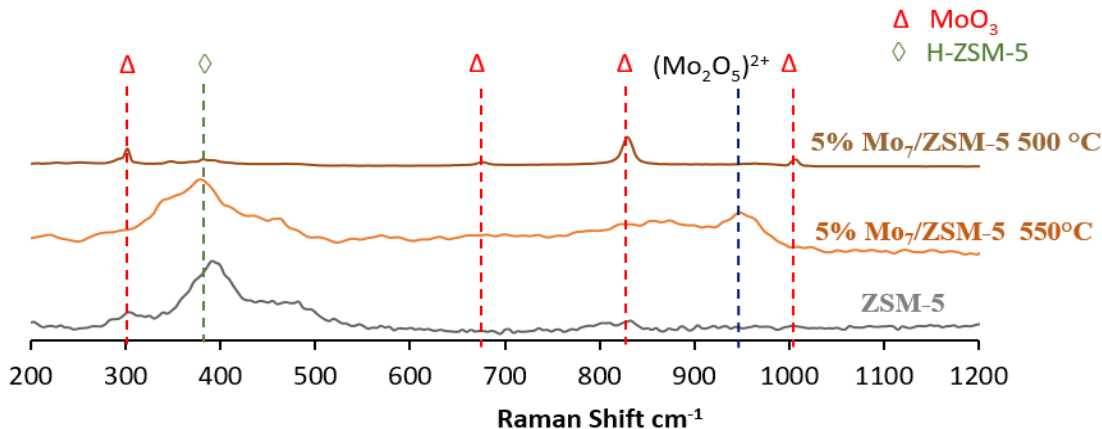
Figure 8. Raman spectra of 5% Mo_7/ZSM-5 catalysts calcined with different temperature

The methane conversion and hydrocarbons yield (benzene, naphthalene and coke) obtained under MNOC reaction at 700ºC (1500 mL/g_{cat}h) by both catalysts are presented in Figure 9.
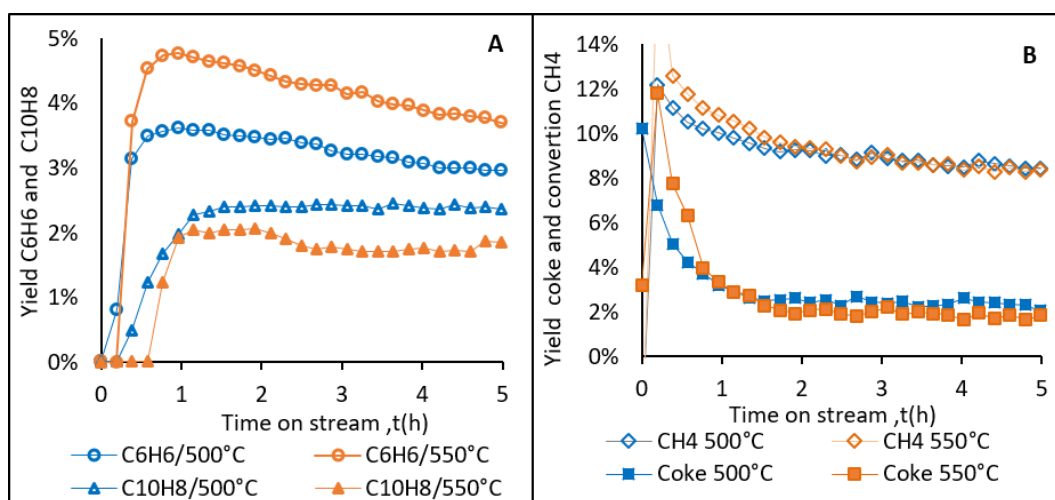
Figure 9. Comparison of the products obtained from 5% Mo_7/ZSM-5 catalysts subjected to different calcination temperatures. **A**. Compare the yield to benzene and naphthalene. **B** Comparison the conversion of methane and yield to the coke formation.

Since the Mo load is the same in both catalysts, the number of active sites for the activation of the methane molecule is expected to be similar in both samples. This would explain their similar methane conversion (Figure 9.B). However, it was found that the sample calcined at 500°C is more selective to the formation of naphthalene and highly dehydrogenated species, i.e. coke, probably due to the different distribution of MoO_x species along the catalysts. As discussed before, in the sample calcined at 500ºC Mo species seem to remain at the catalyst surface. Therefore, the light aromatics (benzene) formed at the catalyst keep on reacting at

the active sites to form polyaromatics (naphthalene) and coke. On the contrary, in the sample calcined at 550ºC the activation of methane takes place mainly within the zeolite channels which act as a molecular sieve limiting the growth of hydrocarbon molecules during oligomerization up to the size of benzene [16] , as it is depicted in Figure 10. For this reason, all the catalysts synthesized in this work for the valorization of methane by non-oxidative coupling were subjected to a calcination temperature of 550°C in advance, in order to improve the yield to benzene (product of interest).
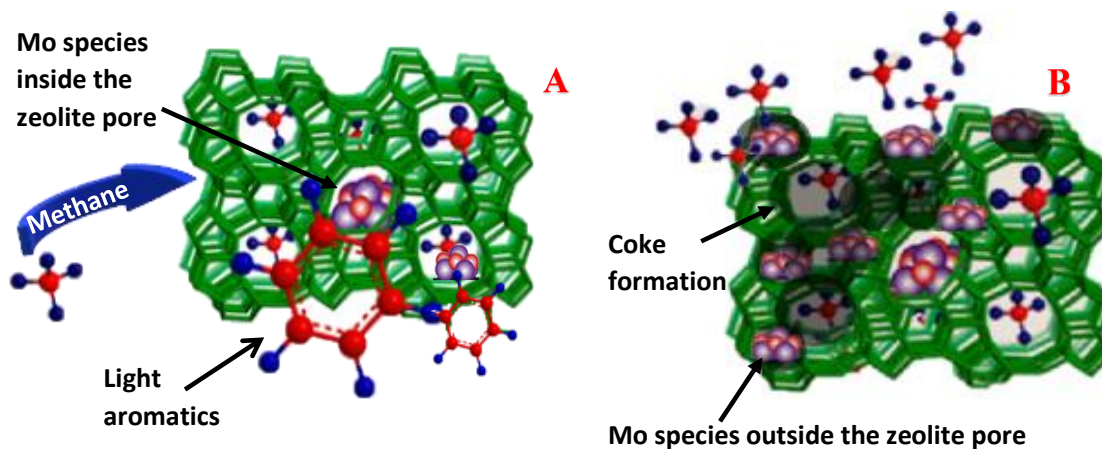

Figure 10. Representation of the reaction at the catalyst synthesized at different calcination temperature. A) 550 °C, B) 500 °C.

4.2. Evaluation of the effect of the Mo precursor type (5% $Mo_{(x)}$/ZSM-5) on the catalyst performance under MNOC

Three different Mo precursors, i.e. the two synthesized POMs (Mo_6 and Mo_8) and commercial salt Mo_7, were tested using ZSM-5 as catalyst support to evaluate their performance under MNOC at the same experimental conditions. As a previous step, a thorough characterization of the samples was carried out.

4.2.1. Catalysts characterization

The formation of the POM structures Mo_6 and Mo_8 was confirmed by Fourier transform infrared spectroscopy (FTIR) analysis (see FTIR spectra and discussion in Annex 1.1, Figure 1). Analogously, XRD diffractograms of fresh ZSM-5 support and 5%Mo_x/ZSM-5 calcined catalysts revealed that the crystalline structure of the zeolite remained unaltered after 5 wt.% Mo loading, regardless the employed precursor (Annex 1.2, Figure 2).

Additionally, a thermogravimetric analysis (TGA) was performed under the experimental conditions described in the Annex 3 to compare the thermal stability of precursors and

catalysts. Figure 11 shows the TGA and DTG curves of the thermal decomposition of the POMs (Mo_6 and Mo_8) and the commercial Mo_7 salt for a temperature range of 50°C–900°C (Figure 11A). The mass loss of these Mo precursors can be attributed to the release of two kinds of water molecules (weak bonded and structurally intercalated crystalline water) and two kinds of ammonium ions (weak bonded and structurally intercalated ammonium ions) associated with the structure of the precursor [17].

It can be observed that the commercial salt shows a very different behavior from that of the POMs (Figure 11A). The TGA and DTG curves of Mo_7 show four mass loss steps (124 °C, 171 °C, 280 °C, and 779 °C) in air. The first one can be assigned to the loss of weakly bonded water molecules from the Mo_7 structure. The second and third mass loss steps are assigned to the evolution of ammonium ions followed by structurally intercalated crystalline water, respectively. The sudden weight loss for the commercial salt Mo_7 at 779 °C or, analogously, the appearance of sharp peak in DTG indicates its sublimation. Meanwhile, the weight loss evidenced in the POMs is related to the loss of volatile components, such as moisture and solvents (tetrabutilammonium ions and water molecules) in the temperature range 250 – 360 ºC.

On the other hand, Figure 11B reveals that, when the precursors are impregnated in the catalyst and calcined their behavior changes. The process begins with a stage associated with the loss of water molecules, both hydration, and coordination. Although the three samples were pre-calcined at 550 ºC, the ZSM-5 support is very hydrophilic and gets normally hydrated from the surrounding atmosphere. In the TGA analysis, the dehydration begins from the first moment in which heat is applied to the sample (around 38 ºC) and extends to temperatures between 120 and 200 ºC. The thermal analysis curves of the catalyst Mo_7/ZSM-5 and Mo_8/ZSM-5 do not show any significant differences, but the physiochemical change in the catalyst Mo_6/ZSM-5 above 550 ºC becomes evident. It suggests that in the pre-calcined Mo_6/ZSM-5 sample at 550 ºC Mo species have not been fully oxidized to MoO_3 and, thus, further interactions of Mo species with the support occur at higher temperatures. Although the employed MNOC reaction temperature is 700 ºC, the preliminary sample heating prior to the catalytic test is always carried out under CH_4:N_2 = 80:20 atmosphere. The different coordination and/or oxidation state of molybdate species among the three samples may impact the proper formation of the active Mo_2C during the

induction period at the beginning of the reaction ($Mo_xO_y + CH_4 \rightarrow Mo_xO_yC_z + H_2O + CO$), thus, leading to eventually different catalytic performance.
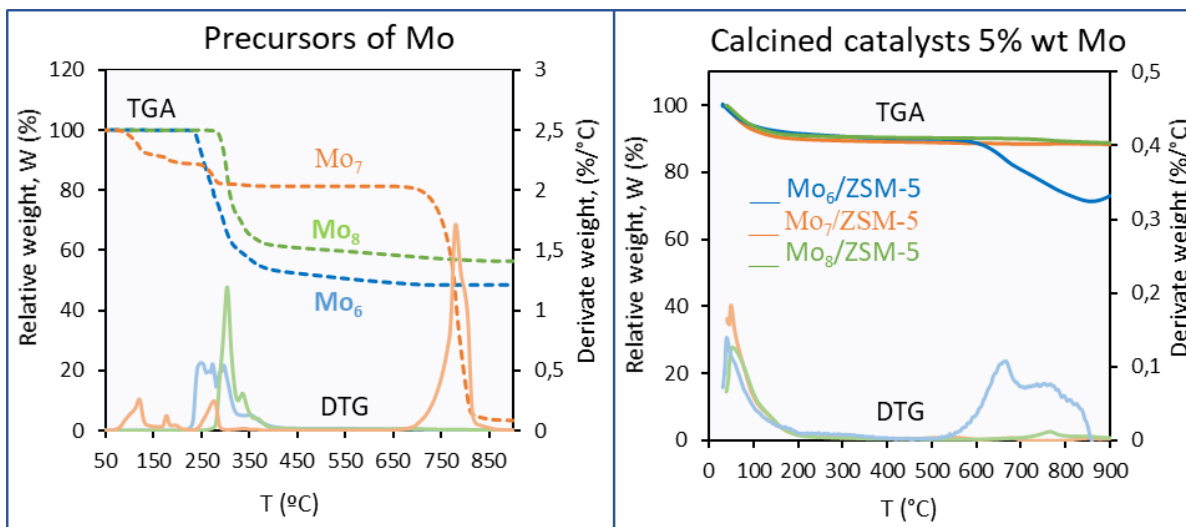

Figure 11. Thermogravimetric analysis of the three precursos Mo_6 Mo_7 and Mo_8. **A)** Precursors of Mo (POMs and commercial salt). **B)** Catalyst calcined

To validate the previous hypothesis, the samples were characterized by XPS (Table 2). This technique qualitatively confirmed that Mo (VI), i.e. MoO_3, was present in all the fresh pre-calcined catalysts, being VI the main Mo oxidation state along the samples. Nevertheless, the presence of Mo (V) in the Mo_6 sample suggests that the incorporation mechanism of Mo differs among the three precursors. After MNOC, however, the metal is reduced to lower oxidation states indicating, for instance, the presence of Mo_2C (related to $Mo^{\delta+}$).

Table 2. Oxidation states of the surfaces of the Mo_x/ZSM-5 catalysts studied in the Mo3d.

Samples		Mo 3d5/2			
		$Mo^{\delta+}$	Mo^{4+}	Mo^{5+}	Mo^{6+}
Fresh	5% Mo_6/ZSM-5			232.1 22%	233.3 78%
	5% Mo_7/ZSM-5			232.0 3%	233.4 97%
	5% Mo_8/ZSM-5				233.0 100%
Coked	5% Mo_6/ZSM-5	229.3 25%	230.7 10%		233.7 65%
	5% Mo_7/ZSM-5	229.0 26%	230.1 12%	232.5 35%	234.0 27%
	5% Mo_8/ZSM-5	229.3 15%	230.4 34%		234.2 51%

In order to gain insight into the MoO_x structures formed at the different samples, Raman spectroscopy characterization was performed to detect the metal-oxide vibrational modes in all these powders. In Figure 15, it can be observed that all samples presented an intense band at 394 cm^{-1} corresponding to the reticular vibration of the zeolite. Additionally, the band at 300 cm^{-1} is attributed to the bending mode of terminal Mo=O and 1003 cm^{-1} to Mo=O stretching mode (only slightly perceived in the catalyst prepared using the Mo_8 octamolybdate precursor). The Mo-O-Mo stretching mode can be observed at 829 cm^{-1}. Finally, it is possible to observe a characteristic peak of $AlMo_6$ entities at 220 cm^{-1}. It seems that all the catalysts with 5% Mo internalize well the characteristic $(Mo_2O_5)^{2+}$ species (dimeric molybdate anchored to the zeolite support, see Figure 12), since all present the band at 960 cm^{-1}. However, the greater intensity of this band in the Mo_6 sample, probably indicates a higher concentration of dimeric molybdate as a result of higher metal dispersion on the support.

This hypothesis was further confirmed by TEM and STEM-EDX. As it can be observed in Figure 13, the bigger the size of the initial polyoxoanion (Mo precursor), the bigger and less disperse is the size of Mo clusters on the zeolite support. The metal dispersion in the $5\%Mo_6$/ZSM-5 is particularly outstanding.
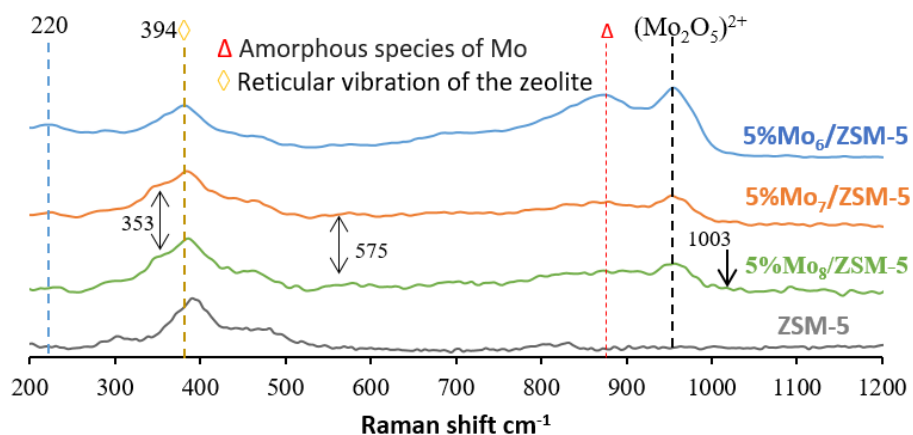

Figure 12. Raman spectrum of catalysts with different Mo precursor at 5% Mo loading.

In agreement with the previous observation, N_2 adsorption measurements indicate that the use of the Mo_6 precursor leads to the smallest pore volume and surface area decrease with respect to the fresh zeolite support and, thus, to the greater metal dispersion (Table 3).

Table 3. Surface area and pore volume properties of Mo/H-ZSM-5 catalysts

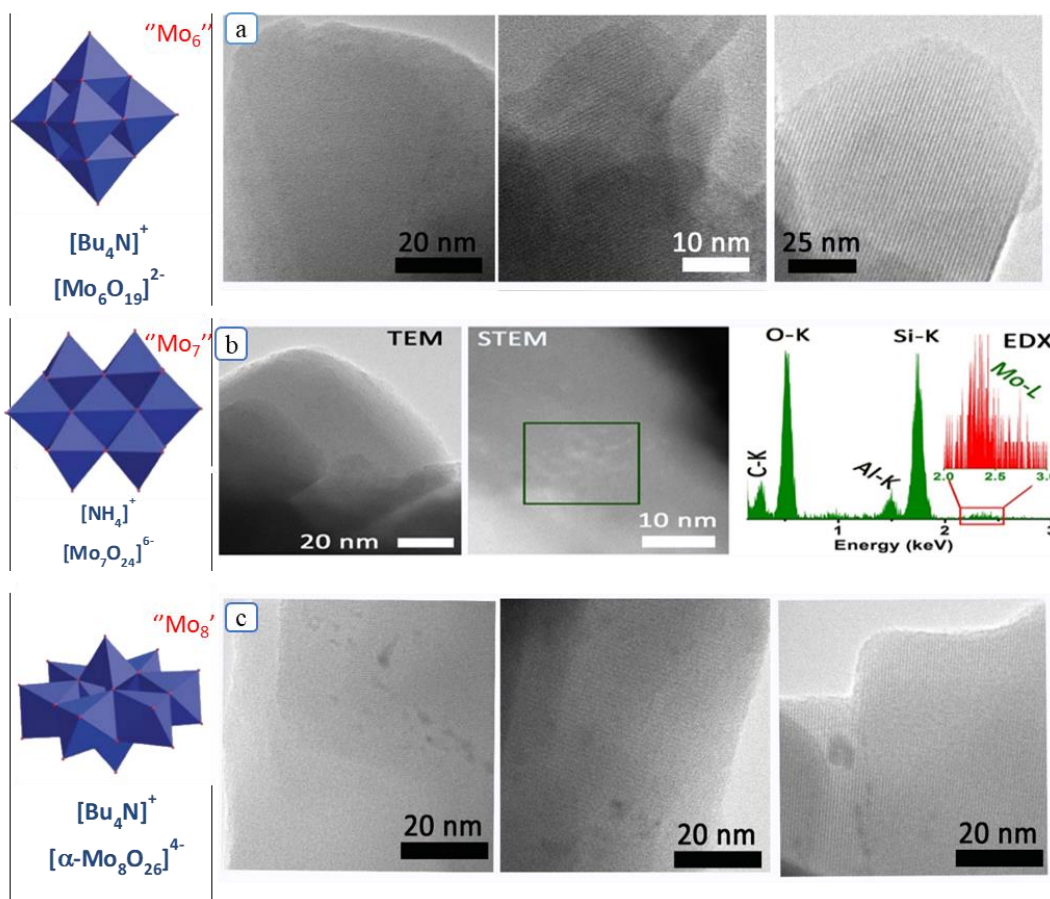| Sample	BET Surface area (m²/g zeolite)	Maximum pore volume at P/Po (cm³/g zeolite)
H-ZSM-5	571 ± 3.6	0.198
5%Mo$_6$/ZSM-5	452 ± 2.1	0.155
5% Mo$_7$/ZSM-5	438 ± 2.4	0.151
5%Mo$_8$/ZSM-5	436 ± 2.6	0.151
5%Mo$_7$/ZSM-5 after reaction	151 ± 0.8	0.052

Figure 13. TEM analysis of catalyst synthesized with different polyoxomolybdate precursors.

4.2.2. *Activity tests of 5% Mox/ZSM-5 catalysts under MNOC*

The catalytic performance of Mo$_x$/ZSM-5 with different POM-based Mo precursors at a load of 5% wt. was tested for methane coupling to higher hydrocarbons under non-

oxidative conditions. The observed products yield and CH_4 conversion results are shown in Figure 14. Mo_x/ZSM-5 catalysts show a bifunctional behaviour for the reaction as the molybdenum species (MoO_xC_y or Mo_2C) activate the C-H bond of methane and the acidic sites of zeolite support help in C_2 formation and further coupling into higher hydrocarbons.
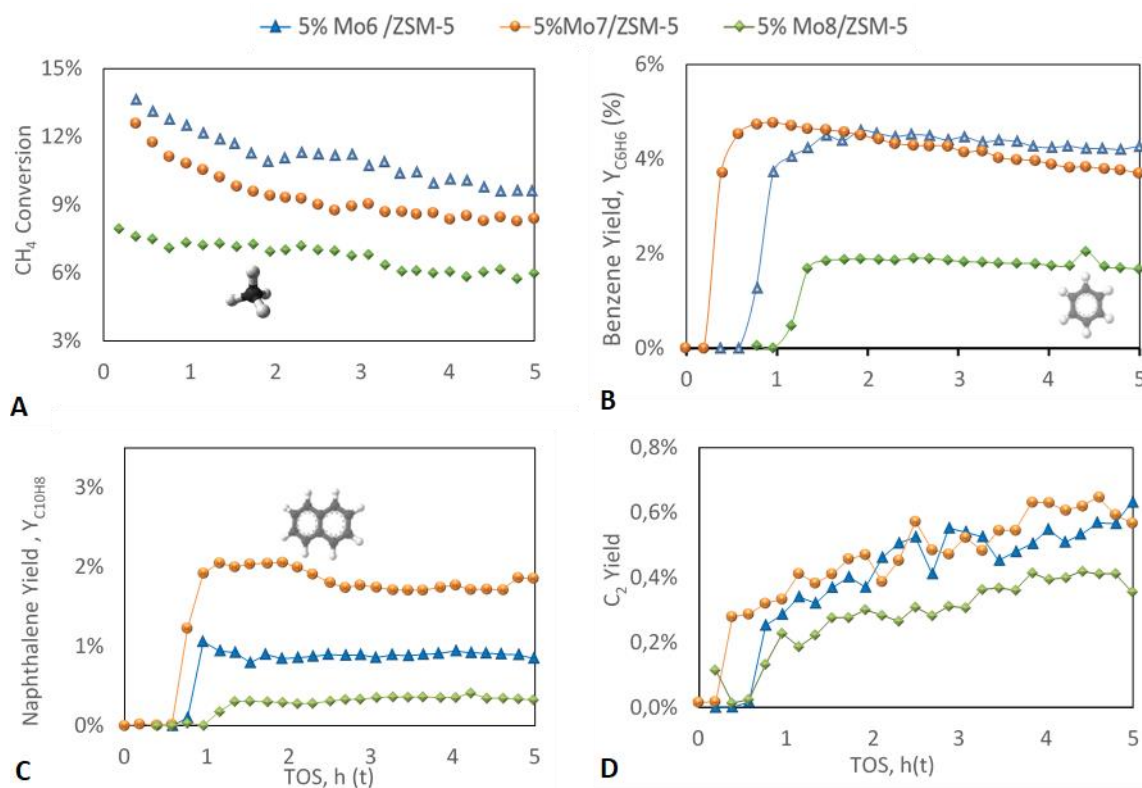

Figure 14. Conversion of methane and aromatics selectivity 5% Mo_x/ZSM-5 using different Mo_6, Mo_7 and Mo_8 precursors. **A)**Methane convertion . **B)** Benzene yield. **C)** Naphthalene yield **D)** C2 (Ethane –ethane) yield**.**

It is observed that the Mo_6/ZSM-5 sample reaches the highest methane conversion among the three catalyst. The different performance is attributed to the different accessibility of CH_4 to the Mo sites depending on their dispersion on the support. Additionally, Mo_7/ZSM-5 catalyst shows the highest initial selectivity to aromatics, i.e. benzene and naphthalene (Figures 14B and 14C). However, this catalyst is not as stable as the Mo_6 sample that, after 3 hours of reaction, shows the highest stable production of benzene being Y_{C6H6} around 4.5%. On the other hand, the Mo_8 precursor shows the lowest CH_4 conversion and, thus, the lowest hydrocarbon productivity. Possibly, this may be because part of Mo remained on the surface of the catalyst (as indicated by its small BET surface and the lower intensity band

of the species $[Mo_2O_5]^{2+}$ in Raman), and has more tendency to coke formation. As a result, the Mo_8 precursor is discarded for the rest of the study. Since both Mo_6 and Mo_7 precursors supported on ZSM-5 performed well under MDA, it was decided to test both precursors on MCM-22 to evaluate the effect of the support on the overall benzene selectivity and catalyst stability.

4.3. Effect of the zeotype support: 5% Mo$_{(6-7)}$/ZSM-5 vs. 5% Mo$_{(6-7)}$/MCM-22

With the aim to increase the selectivity to benzene, we selected a support with a pore size a little smaller than that of the ZSM-5 and very similar to the size of the dynamic diameter of the benzene molecule. Therefore, keeping the same metallic load (5 wt.% Mo), the effect of the change of support to MCM-22 was evaluated with the precursors that showed higher production to benzene: Mo_6 and Mo_7. In this way, it was possible was possible to compare how the change of support (from ZSM-5 to MCM-22) favours the stability and performance of the catalysts, as shown in Figure 15.

It is evidenced that with the change of support, the yield of the production of benzene can be improved. In five hours of reaction, with the catalyst 5% Mo/ZSM-5 a yield of 4.4% C_6H_6 was reached, while with the catalyst 5% Mo/MCM-22 was 6.1%.

It can be seen that independent of the support used to synthesized the catalysts, a higher yield of C_6H_6 and a low yield to $C_{10}H_8$ is always observed for the catalysts synthesized with the Mo_6 precursor compared to the catalysts with the commercial salt Mo_7.

Based on these results, it was decided to work with the 5% Mo$_6$/MCM-22 catalyst that showed the highest percentage of benzene, to determine if increasing the Mo load, we can improve the selectivity and reaction time.
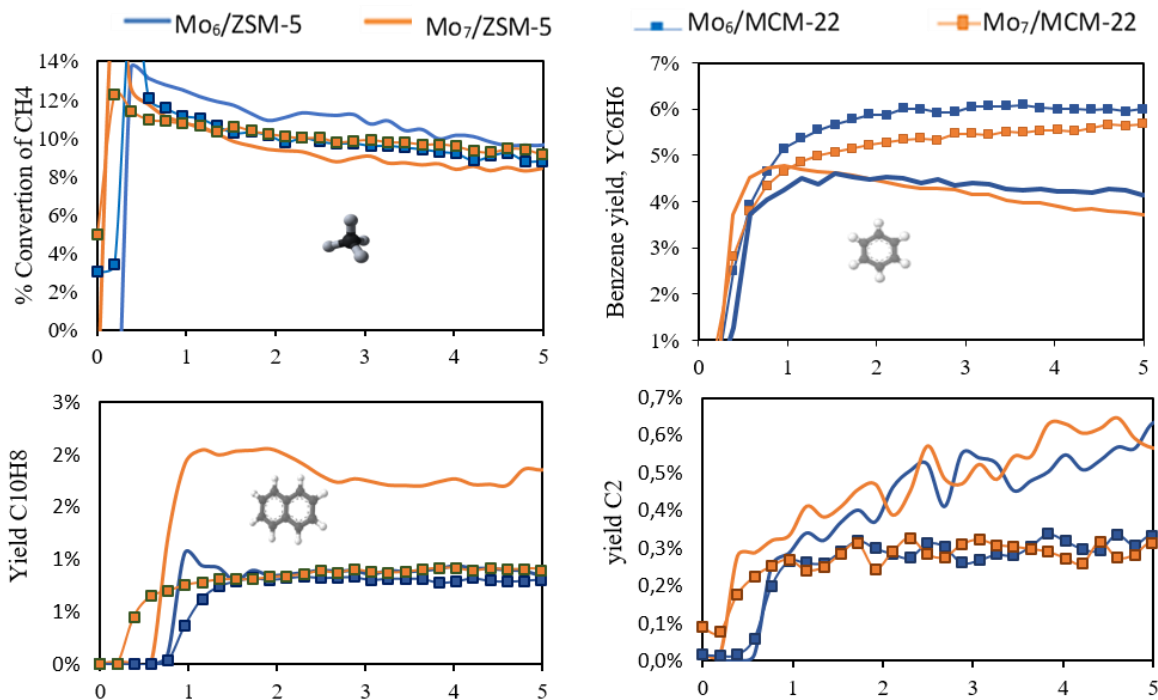
Figure 15. Conversion of methane and aromatics yield of 5% $Mo_{(6-7)}$/ZSM-5 and 5%$Mo_{(6-7)}$/MCM-22 catalysts under MNOC at 700ºC and 1500 mL/g_{cat}h (CH$_4$:N$_2$=80:20). **A)** Methane conversion. **B)** Benzene yield. **C)** Naphthalene yield **D)** C$_2$ (ethane –ethylene-acetylene) yield

4.4. Effect of the Mo load on the x%Mo6/MCM-22 catalytic performance for MNOC

The catalytic performance of Mo_6/MCM-22 catalyst with different Mo loading (5, 8 and 10 wt.%) was tested for methane coupling to higher hydrocarbons under non-oxidative conditions. As a previous step, the three considered samples were fully characterized.

4.4.1. Catalysts characterization

N$_2$ adsorption results (Table 4) illustrate the effect of the metal load on the specific surface and total volume of micropores of the fresh Mo_6/MCM-22 samples. It is observed that both the surface area and the pore volume decrease as the metal load increases. This behavior is related to the accumulation of Mo species formed during the calcination, either as oxides or molybdate dimers, that generate both saturation of the zeolite channels $(Mo_2O_5)^{2+}$ and partial blockage of the pores MoO$_3$ [18], as shown in the conceptual drawing attached to Table 5. The drawing attached to Table 5 illustrates how the Mo load increase results in an increase of MoO$_3$ species on the surface of the catalyst due to the pore saturation. As STEM images indicate that the metal excess accumulates in the form of Mo aggregates on the support surface (Figure 16).

Table 4 . Textural properties of Mo/ZSM-5 catalysts		
Sample	BET Surface area (m² /g zeolite)	Maximum pore volume (cm³/g zeolite)
MCM-22	768 ± 3	0.262
5%Mo$_6$/MCM-22	685 ± 2	0.248
8% Mo$_6$/MCM-22	551 ± 2	0.180

Conceptual diagram of Mo loading in the zeolite

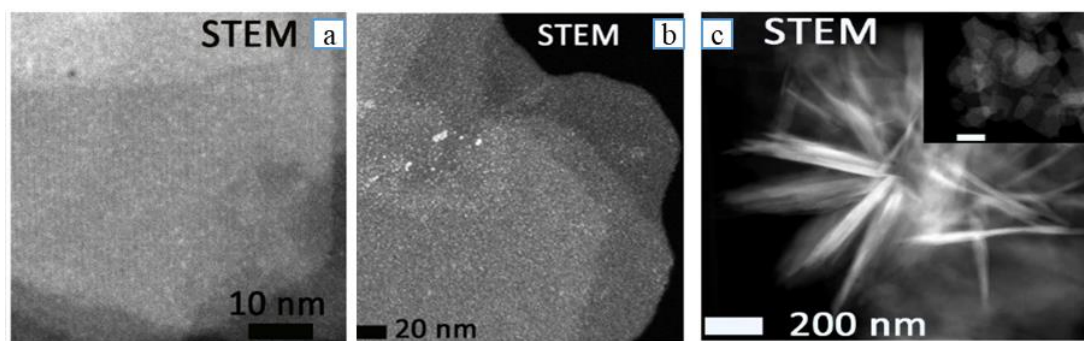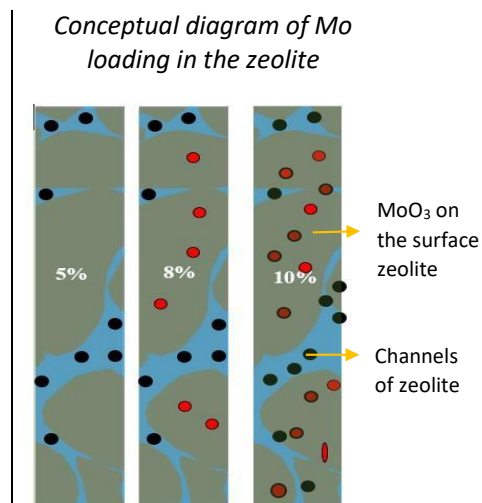MoO$_3$ on the surface zeolite

Channels of zeolite

Figure 16. STEM micrographs. Comparison between 5% Mo$_6$/MCM-22 (a) 8%Mo/MCM-22 (b) and 10% Mo/MCM-22 (c)

STEM images confirm the formation of large external crystals at a load of 8% (Figure 16B) as well as big Mo clusters on the surface of the support at the 10wt.% load (Figure 16C). As it will be shown later, these clusters are supposed to be responsible of both the very high initial catalytic activity and the fast deactivation due to coking of the 10%Mo$_6$/MCM-22 sample.

XRD diffractograms of the three samples confirm the formation of big size external Mo clusters at 8% and 10% Mo load, as revealed by the characteristic MoO$_3$ peak at 23.3° (see Annex 1.4, Figure 3). The 5%Mo/MCM-22 sample, however, does not present diffraction peaks at this angle, thus, indicating well metal dispersion within the MCM-22 pores and unsaturation.

Concerning Raman spectra, new peaks related to crystalline MoO$_3$ appear at X, Y, Z cm^{-1} for the 8% Mo and 10% Mo samples confirming the previous findings. A detailed discussion on the XRD and Raman results for the three considered MCM-22 based

catalysts are found in the Annex 1.5, Figure 4).

4.4.2. *Activity tests of x% Mo₆/MCM-22 catalysts for MNOC*

The catalytic performance of x% Mo_6/MCM-22 with different Mo loads was tested for methane activation to higher hydrocarbons under non-oxidative conditions and the obtained product selectivity and CH_4 conversion results are presented in Figures 17 and 18.
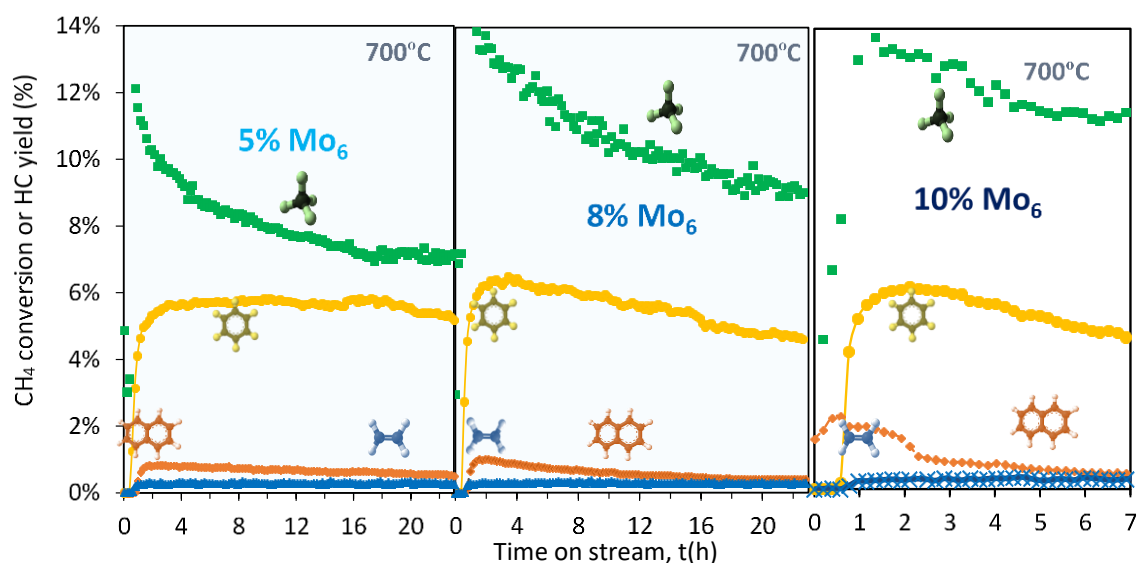

Figure 17. Conversion of methane and aromatics yield obtained for x% Mo_6/MCM-22 catalysts under MNOC using different Mo loadings (5,8,10% wt.). Operational conditions: 700 ℃, 1500 mL/g_{cat}h, CH_4:N_2 = 80:20

As expected, using MCM-22 as support, the selectivity to benzene increased (from 4,4% to 6,1%) with respect to that obtained using the support ZSM-5, (see Figure 15b). Additionally, the reaction stability improved, meaning that the time on stream conversion to benzene could be maintained at ca. 5% for up to 24 h (in the case of the 5% Mo_6/MCM-22 catalyst). The catalyst that shows the best stability and benzene selectivity along the time on stream is the 5% Mo_6/MCM-22, whereby we assumed that 5% is the optimum load for the MCM-22 support like it is concluded in other works [15].

Nonetheless, the 8% Mo_6/MCM-22 catalyst showed a very promising >6 % benzene yield during the first 10 hours on stream, being methane conversion above 10% throughout this period. Although, after this time Y_{C6H6} fell below 6% as a result of catalyst deactivation caused by the formation of coke on the catalyst surface. Concerning the 10% Mo_6/MCM-22 sample, it was found that the catalyst exhibited a high selectivity to aromatics during the first 4 hours of reaction before suffering from fast deactivation due to pore volume decrease by

coke deposition over its active sites. This is related with the formation of large clusters of crystals of MoO_x formed on the surface of catalyst due to the excessive load of Mo that blocked the micropores of MCM-22, as discussed above.

On this regard, we conclude that it is important to maintain the trade-off between Mo loading and acidic sites of zeolite support which is crucial for effective catalyst activity. A combination of the activity of the 8% Mo_6/MCM-22 and the stability of 5% Mo_6/MCM-22 would lead to one of the best catalysts among these reported in literature.
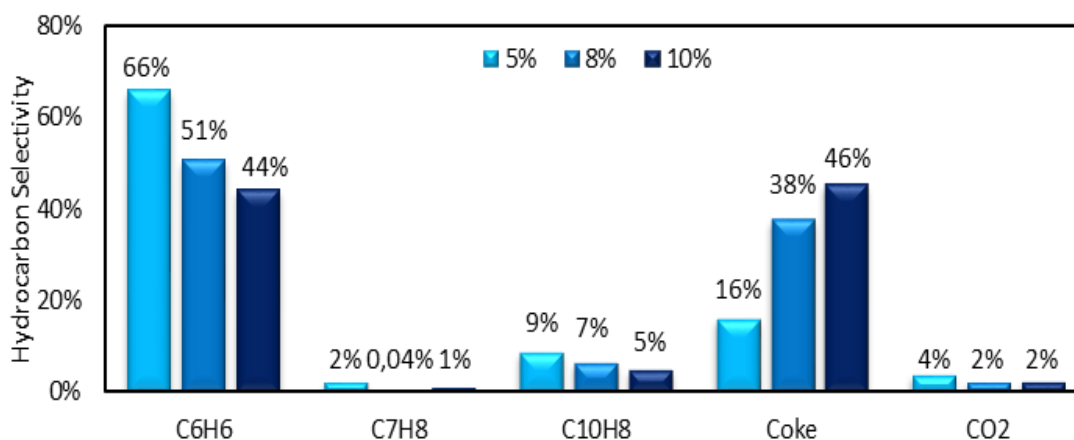

Figure 18. Products selectivity for 5,8,10 wt % Mo_6/MCM-22 catalyst after 5 hours MHA reaction. The catalyst 5% Mo_6/MCM-22 showed a greater selectivity to the formation of aromatics mainly benzene during 22 hours of reaction, like it is showed in figure 19 and 20. Thus, the optimum load for MCM-22 is 5%.

When comparing all the catalysts with different Mo charge at a specific reaction time, i.e. 5 hours from the beginning of the reaction (Figure 18), we observe that the best performance corresponds to the 5% Mo_6/MCM-22 sample. It reaches a compromise between high aromatics selectivity ($S_{C6+} = 75\%$), low coking ($S_{coke} = 16\%$) and moderate methane conversion ($x_{CH4} = 9.2$). In conclusion, in this work we were able to synthesize a catalyst based on MCM-22 zeotype using a polyoxometalate precursor ("Mo_6") that increases both benzene yield and catalytic stability significantly with respect to the highly reported 5% Mo_7/ZSM-5 catalyst for MNOC.

4.5. Results compared with the literature

The following graph has been generated from the optimal benzene production data of the catalysts reported in the literature, comparing these with the best benzene yield obtained in our trials with the 5% Mo_6/MCM-22 catalyst. Literature results are divided into two groups,

i.e. 'pre-Guo' and 'post-Guo'. The well-known work of Guo and co-workers (2014) [16,19-30] represents a breakthrough for the MNOC reaction, as the authors were able to develop a coke-resistant $Fe@SiO_2$ catalyst that provided x_{CH4} up to 42% at 1200ºC. Since then, no one has been able to reproduce this results. This graphic does not provide information about the conversion of the transformation scale of each catalyst or its degree of conversion related to its active centers. Figure 19, only gives an overview of the conversion and selectivity ranges for the process MNOC.

Generally, most of the reports in the literature show an optimal performance of the catalysts after 1-2 hours of reaction, while the catalyst 5% Mo_6/MCM-22 was able to maintain optimal performance values especially to benzene (yield 5.8%) during more than 20 hours of reaction. This shows a substantial improvement of the catalytic stability thanks to the joint effect of the use of MCM-22 and Mo from the precursor based on Mo_6. As it is demonstrated in Figure 19.

In addition to improving the stability of the catalyst in the reaction, it can be seen in Figure 20 that between 16 and 17 hours of reaction can be reached a quasi-free coke reaction regime. The 5% Mo_6/MCM-22 catalyst showed a 92% selectivity to aromatic compounds of which 81% is corresponding to benzene.
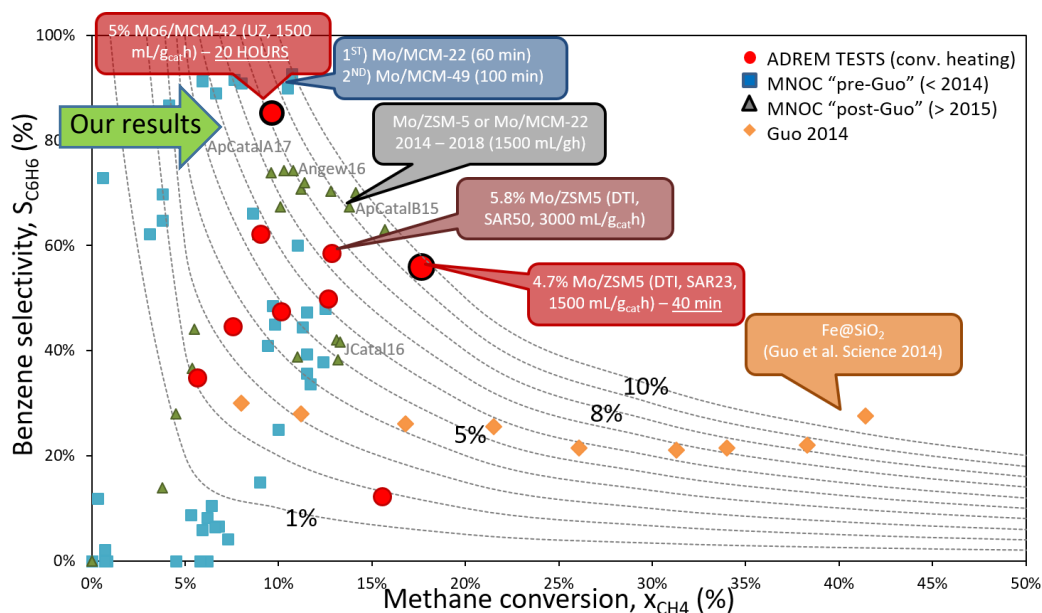

Figure 19. Comparison of benzene selectivity between catalysts reported in the literature and the 5% Mo_6 / MCM-22 catalyst.
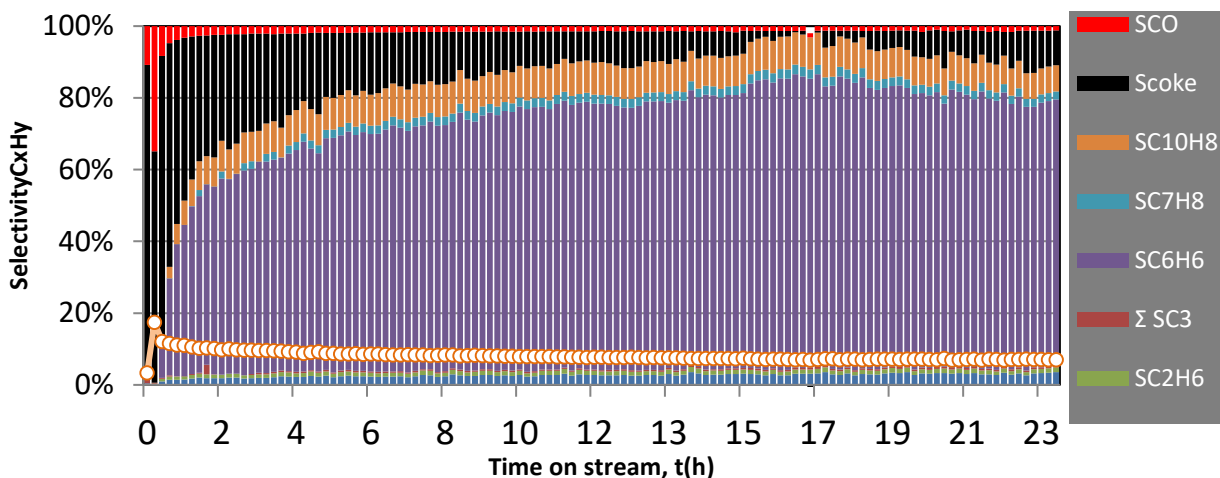
Figure 20. Selectivity of C_xH_y of 5% Mo_6/MCM-22

5. CONCLUSIONS

The dispersion of MoO_x species was found to be the key factor to enhance the catalytic stability of Mo/ZSM-5 and Mo/MCM-22-based catalysts for the non-oxidative coupling of methane. A homogeneous metal load distribution was observed in the case of 5% wt. loading, regardless the zeotype support. Samples with higher metal loads (8 – 10wt.% Mo) did not improve the MNOC process yield towards aromatics, but resulted in the formation of MoO_3 aggregates at the surface of the support that lead to rapid catalyst deactivation. The home-synthesized MCM-22 support outperformed the commercial ZSM-5 zeolite in terms of stability (lower coking) and benzene yield (main product of interest). The Mo precursor based on the polyoxomolybdate $[(C_4H_9)_4N]_2[Mo_6O_{19}]$ "Mo_6" was found to be more active and selective towards benzene than the commercial polyoxomolybdate salt $(NH_3)_6$ $[Mo_7O_{24}]\cdot4H_2O$. This project shows that the catalysts prepared with the "Mo_6" precursor are among the most promising catalysts for methane dehydroaromatization found in the literature. The 5% Mo_6/MCM-22 catalyst displays superior stability (pseudo-steady-state benzene yield for almost 20 hours on stream) and high transient selectivity to aromatic compounds (>75%), working at 700 ºC with a diluted methane flow (CH_4:N_2=80:20) under atmospheric pressure with a spatial velocity of 1500 mL/g_{cat}h.

6. REFERENCES

[1] «ADREM,» [En línea]. Available: https://www.spire2030.eu/adrem. [Ultimo acceso: 08 June 2018].

[2] Liang, F. Y., Ryvak, M., Sayeed, S., & Zhao, N. (2012). The role of natural gas as a primary fuel in the near future, including comparisons of acquisition, transmission and waste handling costs of as with competitive alternatives. Chemistry Central Journal, 6(S1), S4.

[3] Martínez, A., Peris, E., Derewinski, M., & Burkat-Dulak, A. (2011). Improvement of catalyst stability during methane dehydroaromatization (MDA) on Mo/HZSM-5 comprising intracrystalline mesopores. Catalysis today, 169(1), 75-84.

[4] Hu, J., Wu, S., Ma, Y., Yang, X., Li, Z., Liu, H.,& Kan, Q. (2015). Effect of the particle size of MoO3 on the catalytic activity of Mo/ZSM-5 in methane non-oxidative aromatization. New Journal of Chemistry, 39(7), 5459-5469.

[5] Kosinov, N., Coumans, F. J., Li, G., Uslamin, E., Mezari, B., Wijpkema, A. S., ... & Hensen, E. J. (2017). Stable Mo/HZSM-5 methane dehydroaromatization catalysts optimized for high-temperature calcination-regeneration. Journal of Catalysis, 346, 125-133.

[6] Xu, Y., Bao, X., & Lin, L. (2003). Direct conversion of methane under nonoxidative conditions. Journal of Catalysis, 216(1-2), 386-395.

[7] Wang, L., Tao, L., Xie, M., Xu, G., Huang, J., & Xu, Y. (1993). Dehydrogenation and aromatization of methane under non-oxidizing conditions. Catalysis Letters, 21(1-2), 35-41.

[8] Mishra, S., Balyan, S., Pant, K. K., & Haider, M. A. (2017). Non-oxidative conversion of methane into higher hydrocarbons over Mo/MCM-22 catalyst. Journal of Chemical Sciences, 129(11), 1705-1711.

[9] Borrás-Almenar, J. J., Coronado, E., Müller, A., & Pope, M. (Eds.). (2003). Polyoxometalate molecular science (Vol. 98). Springer Science & Business Media

[10] CANCA RUIZ, Jon. Polyoxometalate chemistry: Thermodifractometric study of the dehydration of the compound [Ni ($C_6H_5NO_2$)$_3$]$_2$ [GeW$_{12}$O$_{40}$] · 18 H$_2$O. 2015.

[11] Canca Ruiz, J. (2015). Química de polioxometalatos: Estudio termodifractométrico de la deshidratación del compuesto [Ni ($C_6H_5NO_2$)$_3$]$_2$ [GeW$_{12}$O$_{40}$]· 18 H$_2$O.

[12] Santos Pereda, I. (2016). Química de polioxometalatos.

[13] Corma, A., Corell, C., & Pérez-Pariente, J. (1995). Synthesis and characterization of the MCM-22 zeolite. Zeolites, 15(1), 2-8.

[14] Vuono, D., Pasqua, L., Testa, F., Aiello, R., Fonseca, A., Koranyi, T. I., & Nagy, J. B. (2004). Synthesis and characterization of MCM-22 and MCM-49 zeolites. In Studies in Surface Science and Catalysis (Vol. 154, pp. 203-210). Elsevier.

[15] Julián, I., Ramírez, H., Hueso, J. L., Mallada, R., & Santamaría, J. (2018). Non-oxidative methane conversion in microwave-assisted structured reactors. Chemical Engineering Journal.

[16] Kosinov, N., Coumans, F. J., Uslamin, E. A., Wijpkema, A. S., Mezari, B., & Hensen, E. J. (2016). Methane dehydroaromatization by Mo/HZSM-5: mono-or bifunctional catalysis? ACS Catalysis, 7(1), 520-529.

[17] Chithambararaj, A., Mathi, D. B., Yogamalar, N. R., & Bose, A. C. (2015). Structural evolution and phase transition of $[NH_4]$ $6Mo_7O_{24}$. $4H_2O$ to 2D layered MoO_3- x. Materials Research Express, 2(5), 055004.

[18] Ma, D., Shu, Y., Han, X., Liu, X., Xu, Y., & Bao, X. (2001). Mo/HMCM-22 catalysts for methane dehydroaromatization: a multinuclear MAS NMR study. The Journal of Physical Chemistry B, 105(9), 1786-1793

[19]Tempelman, C. H., & Hensen, E. J. (2015). On the deactivation of Mo/HZSM-5 in the methane dehydroaromatization reaction. Applied Catalysis B: Environmental, 176, 731-739.

[20] Rahman, M., Sridhar, A., & Khatib, S. J. (2018). Impact of the presence of Mo carbide species prepared ex situ in Mo/HZSM-5 on the catalytic properties in methane aromatization. Applied Catalysis A: General, 558, 67-80

[21] Kosinov, N., Coumans, F. J., Uslamin, E., Kapteijn, F., & Hensen, E. J. (2016). Selective coke combustion by oxygen pulsing during Mo/ZSM-5-catalyzed methane dehydroaromatization. Angewandte Chemie International Edition, 55(48), 15086-15090.

[22] Zhang, Y., Kidder, M., Ruther, R. E., Nanda, J., Foo, G. S., Wu, Z., & Narula, C. K. (2016). Promotional Effects of In on Non-Oxidative Methane Transformation Over Mo-ZSM-5. Catalysis Letters, 146(10), 1903-1909.

[23] Zhang, C. L., Li, S., Yuan, Y., Zhang, W. X., Wu, T. H., & LIn, L. W. (1998). Aromatization of methane in the absence of oxygen over Mo-based catalysts supported on different types of zeolites. Catalysis letters, 56(4), 207-213.

[24] Wang, K., Huang, X., & Li, D. (2018). Hollow ZSM-5 zeolite grass ball catalyst in methane dehydroaromatization: One-step synthesis and the exceptional catalytic performance. Applied Catalysis A: General, 556, 10-19

[25] Liu, H., Yang, S., Hu, J., Shang, F., Li, Z., Xu, C., ... & Kan, Q. (2012). A comparison study of mesoporous Mo/H-ZSM-5 and conventional Mo/H-ZSM-5 catalysts in methane non-oxidative aromatization. Fuel processing technology, 96, 195-202.

[26] Wang, D. Y., Kan, Q. B., Xu, N., Wu, P., & Wu, T. H. (2004). Study on methane aromatization over MoO3/HMCM-49 catalyst. Catalysis today, 93, 75-80.

[27] Liu, L., Ma, D., Chen, H., Zheng, H., Cheng, M., Xu, Y., & Bao, X. (2006). Methane dehydroaromatization on Mo/HMCM-22 catalysts: effect of SiO 2/Al 2 O 3 ratio of HMCM-22 zeolite supports. Catalysis letters, 108(1-2), 25-30.

[28] Tan, P. (2018). The catalytic performance of Mo-impregnated HZSM-5 zeolite in CH4 aromatization: Strong influence of Mo loading and pretreatment conditions. Catalysis Communications, 103, 101-104.

[29] Tan, P. (2016). Active phase, catalytic activity, and induction period of Fe/zeolite material in nonoxidative aromatization of methane. Journal of Catalysis, 338, 21-29.

[30] Yin, X., Chu, N., Yang, J., Wang, J., & Li, Z. (2014). Synthesis of the nanosized MCM-22 zeolite and its catalytic performance in methane dehydro-aromatization reaction. Catalysis Communications, 43, 218-222.

ANNEXES

1. Complementary results

1.1. POMs characterization. FTIR

The main characteristic peaks of each of the POMs were identified. The infrared of this type of compounds appear at wave numbers less than 1100 cm-1. The symmetric and anti-symmetric vibrations of the different Mo-O bond types are observed in the following regions: 1000-920 cm-1 for the voltage vibration of the Mo=O link (terminal oxygen); 900-770 cm-1 for the voltage vibration of the Mo-O-Mo bridge (oxygen of two octahedrons that share a vertex); 810-700 cm-1 for the voltage vibration of the Mo-O-Mo bridge (two-octahedron oxygens that share edge). For the POM Mo_8, it is observed a strong peak at 808 cm-1 that is characteristic for the α-isomer.
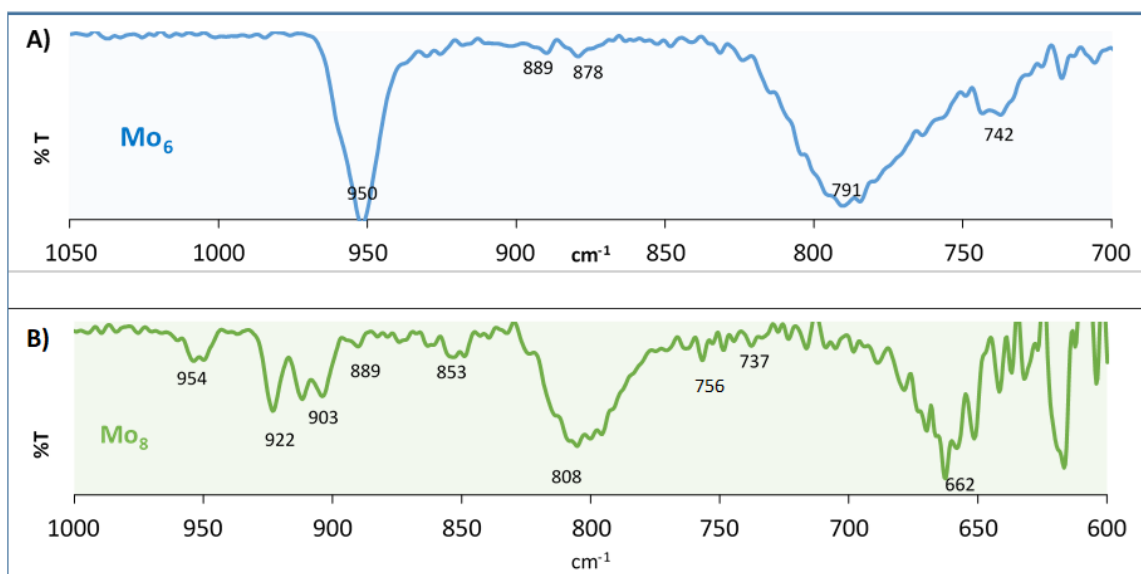

Figure 1. FTIR of A) Tetrabutylammonium hexamolybdate (VI) $[Bu_4N]_2 [Mo_6O_{19}]$ "Mo_6" B) Tetrabutylammonium octamolybdate (VI) $[Bu_4N]_4 [Mo_8O_{26}]$ "Mo_8".

1.2. XRD patterns of ZSM-5 fresh and Mo/ZSM-5 catalysts prepared with different

Figure 2 shows the XRD of the catalysts calcined with the three precursors of Mo in zeolite ZSM-5. The main diffraction peaks between 20 ° and 25 ° correspond to the pattern structure

of the zeolite and were observed for all Mo/ZSM-5 samples, there is no significant change of the zeolite framework by the addition of molybdenum species. Nevertheless, their lower intensity with respect to these of the fresh zeolite indicates crystallinity loss as a result of cationic exchange of Mo species with the zeolite protons.
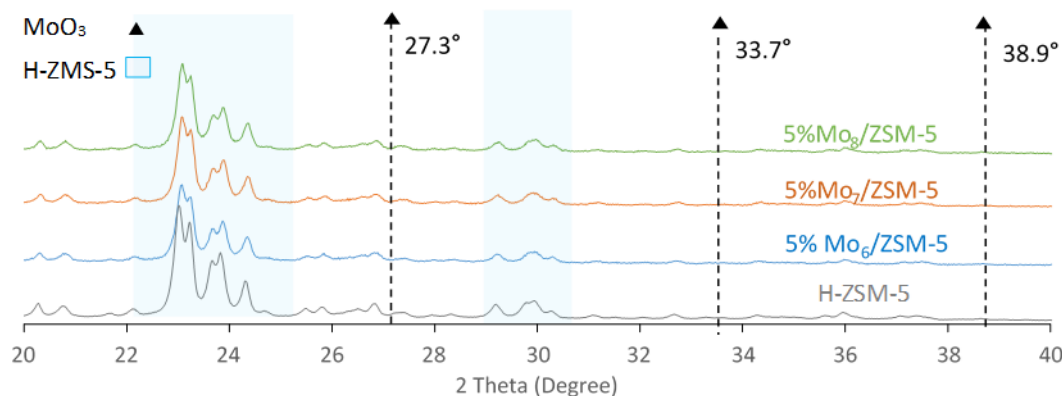

Figure 2. XRD patterns of ZSM-5 fresh and Mo/ZSM-5 catalysts prepared with different molybdenum precursors

The peaks at 27.3°, 33.7° and 38.9° are the characteristics to identify species of MoO_3 that are formed on the zeolite, these peaks at Mo loading concentrations of 5% wt., could be not detected, indicating that crystalline domains of molybdenum oxide formed were below the detection limit of the equipment and did no show specific reflections. Besides, this suggests a good dispersion of the molybdenum oxide species on the zeolite surface [2], that were confirmed through TEM analysis, (see figure 13 in the session 4.2).

1.3. XRD Mo6/HMCM-22 catalysts with 5, 8, and 10 wt% loading of Mo

Figure 3 shows the XRD pattern of the calcined catalysts with different % Mo loading of the Mo6 precursor over the MCM-22 support. From the data it can be deduced that there is not much change in the XRD pattern of the zeolite after Mo loading, suggesting that molybdenum does not affect the channel framework and crystallinity of the support; however, the intensity of the HMCM-22 zeolite peaks decreases slightly upon increasing % Mo loading. The XRD pattern of 5% Mo6/MCM-22 A shows a low concentration of Mo(VI) species due to Mo migration into the zeolitic pores, but upon increasing the load of molybdenum to 8 and 10%, some peaks of MoO3 species are evident in the XRD pattern of these catalysts, for example at diffraction angle 23.3°.
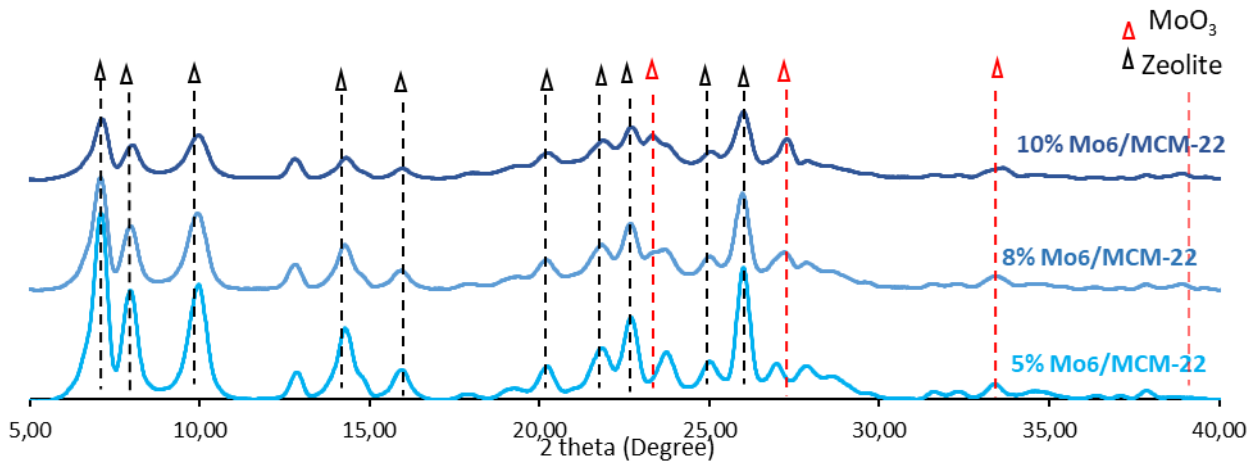
Figure 3. XRD Mo$_6$/HMCM-22 catalysts with 5, 8, and 10 wt% loading of Mo

1.4. Raman spectra of the catalysts Mo6/HMCM-49 with different load of Mo.

Figure 4, shows the Raman spectra of the calcined catalysts x% Mo$_6$/MCM-22. The band observed at 965 cm^{-1} corresponds to the MoOx species grafted onto the MCM-22 channel in Al sites similar to the published literature [Ref **]. This demonstrates that an interaction between molybdenum and the zeolite lattice occurred during the calcination process of the catalysts when Mo migrates into the channels of the zeolite and reacts with bridging hydroxyls groups, as shown in Figure 2. Thus, Mo is anchored to the framework Al through an oxide bridge, so it modifies the acidic properties of the MCM-22 and leads to a high dispersion of the molybdenum [8]. As the wt% Mo in the catalysts is increased, the intensity of their peaks increases. Furthermore, the catalysts loaded at 8 and 10% Mo show the appearance of new peaks, not present in the 6% Mo loading.
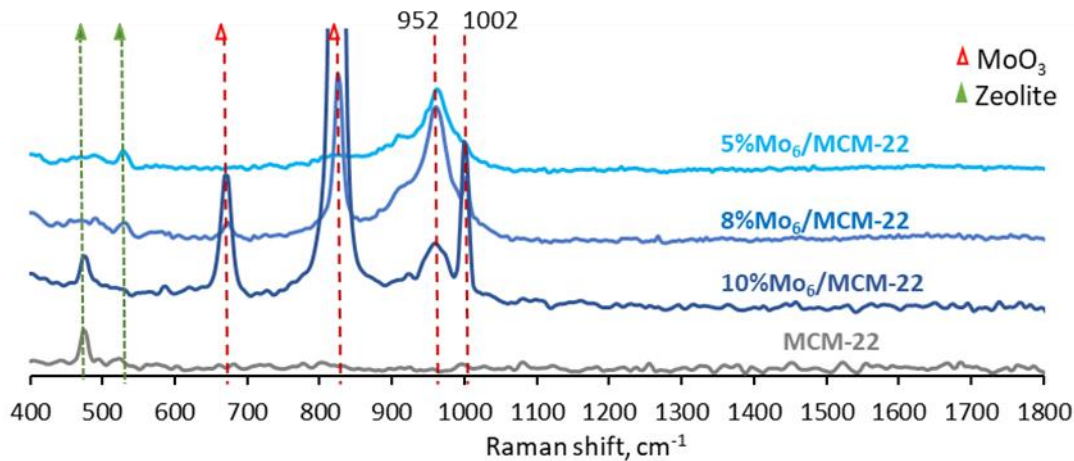
Figure 4. Raman spectra of the catalysts Mo_6/HMCM-49 with 5, 8, and 10 wt.% of Mo

2. Future work in this project include:

•Perform temperature programmed desorption of pyridine (TPD-pyridine) analysis, in order to determine the total number of acidic sites at each catalyst.

•Measure the catalytic activity of the synthesized catalyst 5%Mo_6/MCM-22 in a catalytic reactor assisted by microwave (MW) heating. The catalyst should be tested either in powder form or supported on MW-sensitive structured monoliths, e.g. SiC honeycombs.

•Develop and optimize a suitable catalyst slurry formulation for monolith coating.

•Evaluate the catalyst effectiveness for methane conversion and aromatics production with respect to that obtained under conventional heating.